UNIVERSITA' POLITECNICA DELLE MARCHE
FACULTY OF ENGINEERING

Master's Degree Course ***GREEN INDUSTRIAL ENGINEERING***

Simulation and Modelling of Organic Rankine Cycle and Absorption Chiller Processes for Cooling Requirements Integrated with Ferrara Medium Enthalpy Geothermal System and Utilizing the Best Process to Design a Data Center

Supervisor:

Prof. Gabriele Comodi

Co-supervisor(s):

Prof. Marco Taussi

Candidate:

Hilal Jbara

A.Y. 2025/2026

Acknowledgement

I want to extend my sincere gratitude and appreciation to everyone who helped finish my thesis. Their Encouragement, advice, and support have been crucial during this difficult yet rewarding path

First and foremost, I want to express my sincere gratitude to my supervisors at Saipem, Geothermal Energy Product Manager **Mariella Leporini** for giving me the opportunity to carry out this work within the company and Senior Researcher **Mauro Fehervari**, for his assistance. Their professional support, technical insights, and constant encouragement greatly enriched this research and provided me with a valuable practical perspective.

Also, I owe a dept of gratitude to my academic supervisors, **Prof. Gabriel Comodi** and **Prof. Marco Taussi**, for their valuable guidance, continuous support, and constructive feedback throughout the development of this thesis. Their expertise and availability were fundamental in shaping both the scientific content and the overall quality of this work.

Finally, I would like to acknowledge my family, whose steadfast presence has accompanied me throughout my academic path. Their quiet sacrifices, moral support, and unyielding confidence in my goals provided the stability and encouragement necessary to overcome difficulties and remain focused during the most demanding phases of this journey.

Abstract

The swift expansion of data centers has resulted in a significant increase in electricity usage, with cooling accounting for a large portion of overall energy consumption. This research examines the incorporation of medium-enthalpy geothermal energy from the Ferrara geothermal system (Italy) to aid in the design of an eco-friendly data center with minimized environmental effects. The geothermal resource offers around 14 MW of thermal energy at 100 °C, ideal for energy conversion systems.

A comparative evaluation of two geothermal utilization methods was initially performed: (1) an Organic Rankine Cycle (ORC) producing electricity to power standard electric chillers, and (2) a direct Lithium Bromide–Water (LiBr–H_2O) absorption chiller powered by geothermal energy. The cooling capacity and thermodynamic performance of both systems were assessed by modelling them with Aspen HYSYS and Aspen Plus.

According to the comparison, the LiBr absorption chiller exhibited better performance, providing significantly more useful cooling by directly utilizing thermal energy and minimizing various conversion losses. Also environmental assessment shows substantial decreases in indirect CO_2 emissions and removal of high-GWP refrigerants. As a result, a conceptual design for a data center in the Ferrara region was created utilizing a geothermal-driven absorption cooling system. This confirms that direct geothermal absorption cooling is the most effective and sustainable method for integrating geothermal power in data centers. As assumed, integration of geothermal energy with data centers cooling processes will help in reducing the Power Usage Effectiveness of the data center, thus reducing the annual energy consumption and CO_2 emissions.

Table of Contents

List of Figures

List of Tables

List of Abbreviations

Chapter 1: Introduction

The increasing demand for digital services has led to rapid growth in data centers worldwide, resulting in significant energy consumption and associated environmental impacts. Among the various energy requirements of data centers, cooling systems represent one of the largest contributors to overall electricity consumption. Consequently, the development of sustainable and energy-efficient cooling solutions has become a critical research area in the context of energy transition and decarbonization strategies.

Geothermal energy offers a reliable and renewable source of thermal energy that can be exploited for heating and cooling applications. Medium-enthalpy geothermal resources provide opportunities for integrating thermodynamic cycles capable of converting thermal energy into useful cooling capacity. The Ferrara geothermal system represents a valuable case study due to its established infrastructure and availability of geothermal resources suitable for energy conversion processes.

This thesis investigates the potential integration of two alternative technologies—the Organic Rankine Cycle (ORC) and the Absorption Chiller Cycle (AC)—with the Ferrara medium-enthalpy geothermal system to satisfy cooling requirements for data center applications. The study focuses on the modelling and simulation of both processes, aiming to evaluate their thermodynamic performance, energy efficiency, and suitability for supporting sustainable data center operation.

1.1 Geothermal Energy

Geothermal Energy utilizes the thermal energy contained in rocks and fluids located in the Earth's crust. The source of this heat is associated with the radioactive processes and the continuous release of primordial heat occurring at the inner parts of our planet , which make geothermics a renewable energy source. Although this heat exists in vast, nearly limitless amounts in the Earth's crust and the deeper layers of the planet, it is distributed unevenly, rarely found in concentrated forms, and frequently located at depths unsuitable for industrial extraction. The World used about 200 TWh of direct geothermal heat in 2023 and generated roughly 97 TWh of electricity from geothermal sources in 2022 [1].

Nowadays, geothermal energy meets less than 1% of global energy demand and its use is concentrated in a few countries with easily accessible and high-quality resources [2]. With continued technological improvements and reductions in project costs, geothermal could meet up to 15% of global electricity demand growth to 2050 [2]. The technical potential of geothermal would be enough to meet both electricity and thermal demand in Africa, China, Europe, Southeast Asia and the United States [2]. Increasing recognition of geothermal potential coincides with a period when global electricity demand is poised to surge due to traditional applications, like cooling, as well as emerging ones, including electric vehicles and data centers. The presence of geothermal energy would be especially beneficial for enhancing electricity security.

Muffler & Cataldi (1978) categorized geothermal systems according to reservoir temperature into high (> 150 °C), medium (90 to 150 °C), and low temperature (<90 °C). From now on, the collective terms "low- to medium-temperature" will refer to temperatures under 150 °C. Recently, it is stated that systems operating at low- to medium-temperature are significantly more widespread than high temperature ones [3]. The following *Table 1* shows the advantages and disadvantages of geothermal energy.

Table 1. Advantages and disadvantages of Geothermal Energy

Advantages	**Disadvantages**
Renewable and sustainable	Location-specific

Low greenhouse gas emissions	High costs for drilling and setup
Reliable and stable (baseload energy)	Risk of induced seismicity
Small land footprint	Resource depletion if poorly managed
Reduces dependence on imported fuels	Water disposal (if not reinjected)

1.2 Industries that can be integrated with Geothermal Energy

Geothermal systems are expected to find a wide range of applications in many industries soon. It will be important in reducing carbon and greenhouse gases emissions, satisfying energy demands, and encouraging sustainable development in various sectors as technology develops and the value of Renewable Energy rises. The Geothermal Energy market report mentioned that in 2021 GE was valued at $6.6 billion, and it is expected to achieve a market size of $9.4 billion by 2027, with a projected annual growth of 6% per year [4].

Energy generation continues to be the primary use, with worldwide geothermal power capacity hitting 15.96 GW in 2021, increasing at approximately 3.5% each year, whereas heating and cooling applications reached 107 GWh in 2020, growing at an annual rate of 9% [5].Geothermal energy provides a flexible and sustainable thermal resource that can be incorporated into various industrial sectors *(Figure 1)*. In the water industry, geothermal energy aids desalination and water purification processes, lowering energy expenses for distillation and evaporation. The technology sector, encompassing data centers, is progressively utilizing geothermal energy for electricity generation and cooling, capitalizing on its consistent temperatures to enhance server performance. The chemical sector utilizes geothermal heat for operations like drying, evaporation, and mineral extraction, whereas the manufacturing of construction materials (cement, bricks) and the wood and steel sectors employ geothermal for preheating and drying, lowering reliance on fossil fuels. Ultimately, district heating and cooling (DHC) represents a significant growth sector, with forecasts estimating 17,500 geothermal district heating systems by 2050 and 28 million geothermal heat pump installations in the U.S. by that time, as reported by NLR [6]. These integrations not only lower operational expenses but also decrease CO_2 emissions by 50–70% relative to fossil-based systems, establishing geothermal as a fundamental element for industrial decarbonization [7].

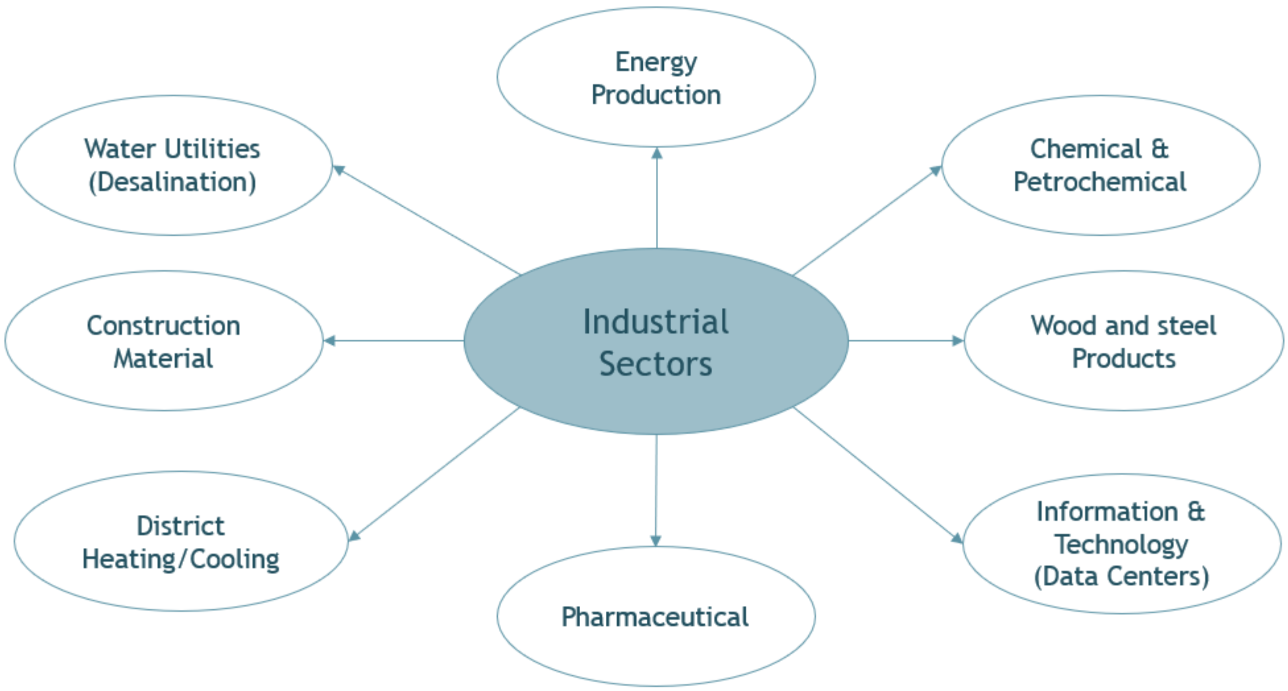

Figure 1. Industries that can be integrated with geothermal energy

1.3 Energy-Intensive Industries

Energy-intensive industries are sectors that require substantial energy per unit of production, mainly because of their processes. These sectors are crucial for economic growth yet account for a significant portion of worldwide energy use and greenhouse gas emissions. The International Energy Agency (IEA) states that over 75% of global industrial energy consumption comes from energy-intensive industries [8].

Also, because their processes include high temperatures, heavy machinery, and continuous operation, energy-intensive industries like steel, cement, chemicals, and paper manufacture demand a lot of energy. For instance, chemical manufacture frequently relies on energy-intensive reactions and separation procedures, but the production of steel or cement requires furnaces that run at extremely high temperatures. To satisfy worldwide demand, these sectors likewise operate on a massive scale, which raises their energy consumption even further. They so contribute significantly to the total amount of energy used in industry and are important in conversations about sustainability and energy efficiency. In this case, energy-intensive applications including desalination systems, data centers, and district heating and cooling infrastructure, are the focus. Data centers need a high amount of energy to run computers and use sophisticated cooling systems to maintain ideal temperatures, while district heating and cooling networks use energy to effectively distribute the warm-hot fluid throughout buildings. On the other hand, desalination operations use methods like thermal distillation or reverse osmosis to separate salt from seawater, they are also quite energy intensive because of the separation processes. These industries are essential for increasing energy efficiency and incorporating sustainable solutions.

The industrial sector uses approximately 54% of the global delivered energy, mainly for heating and cooling processes [9]. Moreover, these sectors show significant electricity and heat usage, positioning them as primary contributors to worldwide energy needs and carbon output. Figure 2 shows the requirements and deliveries of energy intensive industries.

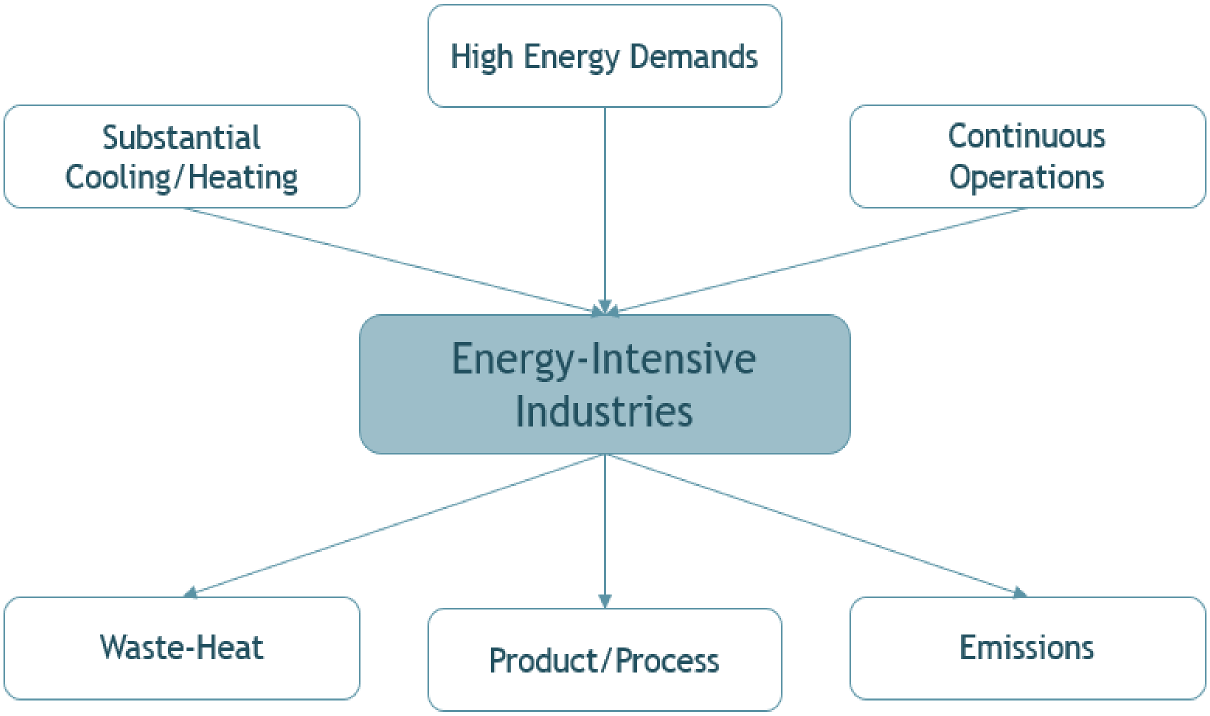

Figure 2. Requirements and deliveries of energy-intensive industries

1.3.1 Data Centers and Computing Infrastructure

Data centers rank as some of the quickest expanding energy users worldwide because of the rapid increase in cloud computing, artificial intelligence, and digital services. As nearly all the energy consumed by servers transforms into heat, it results in the release of hundreds of TWh of energy in the form of heat each year. Data center infrastructure encompasses the assortment of physical and virtual assets that facilitate the functioning of a company's computing ecosystem. It generally consists of elements like servers, storage devices, networking hardware, and data cables, along with power and cooling systems to maintain these components at ideal temperatures [10]. This infrastructure is essential for the effectiveness, safety, and dependability of data processing, storage, and distribution within an organization.

In 2024, data centers consumed approximately 415 TWh, representing about 1.5% of global electricity demand. Projections indicate that this consumption could increase at an annual growth on the order of 10–15% per year in the latter 2020s, reaching up to 945

TWh by 2030, largely driven by AI workloads, larger sites, and higher utilization rates [11] (*Figure 3*). Indeed, average new facilities skew above 100 MW, with ~25% of planned sites at ≥500 MW, and some exceeding 1 GW [12].

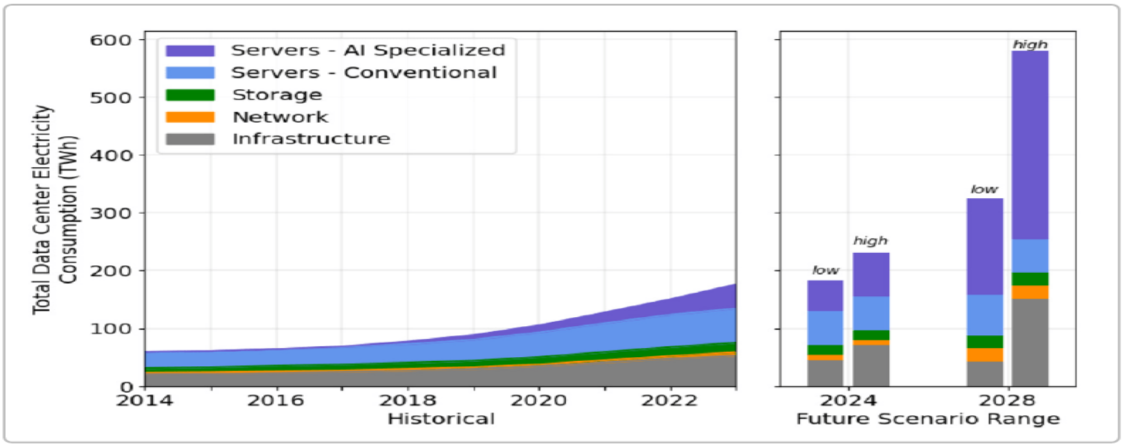

Figure 3. Historical and future estimated increase in electricity consumption of data centers [10]

From an environmental point of view, the average carbon footprint of data centers decreased from 366.9 Mt CO_2e/GWh in 2019 to 312.7 Mt CO_2e/GWh in 2024 (*Figure 4*), due to the increase in renewable energy use [13]. Data centers use different water sources for cooling, with potable water subjected to human consumption still playing a major role due to its reliability, accounting for about 57–65% of use [14]. Recently, a growing shift toward reclaimed or recycled water occurred, whit the latter already used in over 25% of facilities to improve sustainability [15]. In addition to that, surface and groundwater sources can represent a significant share, reaching up to 80–90% of withdrawals in certain cases [16], while alternative sources like seawater or rainwater remain limited, even though they are gradually increasing in adoption. The global data center market was valued at $347.6 billion in 2024 and is projected to reach $652.01 billion by 2030, growing at a CAGR of 11.2% from 2025 to 2030 [17].

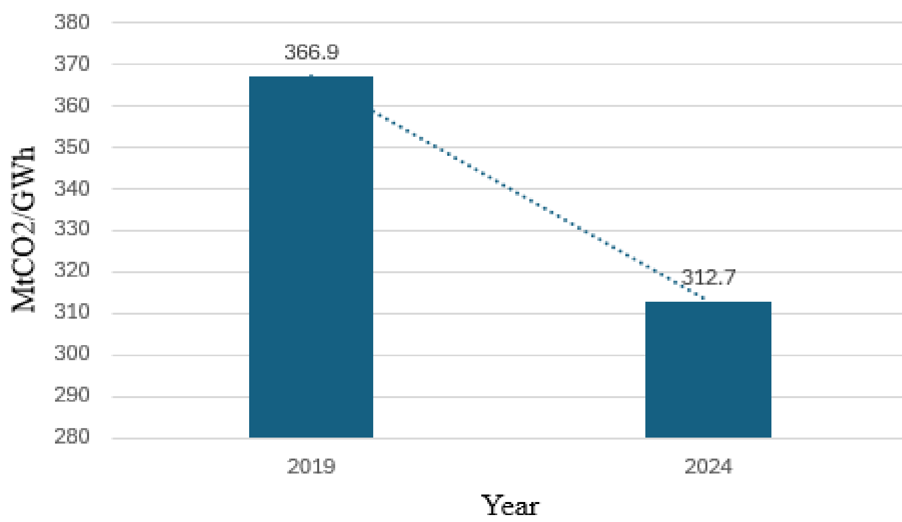

Figure 4. Evolution amount of CO2 emitted by Data Centers from 2019 to 2024.

1.3.2 Large District Heating and Cooling Networks

District Heating and Cooling (DHC) networks are centralized energy systems designed to supply thermal energy, hot water, steam, or chilled water from a central plant to several commercial, residential or industrial complexes, through insulated pipes [18]. Heating and cooling represent nearly 50% of the world's final energy use. It represents the biggest source of energy consumption and accounts for over 40% of carbon dioxide emissions worldwide linked to energy [19]. The global DHC market was valued at $210.35 billion in 2024 and is projected to reach $274.74 billion by 2033, growing at a CAGR of 9.31% [20].

In 2022, the heat generated for global district heating networks was approximately 17 EJ which is equal to 17×10^{18} Joules, comparable to 2021, but roughly 10% higher than 2020 and 17% greater than the ten previous years [18]. DH presently fulfills approximately 9% of worldwide heating needs, yet nearly 90% of its energy is sourced from fossil fuels. In 2022, CO_2 emissions from district heating production rose by 1.5% compared to 2021 and were approximately 25% greater than in 2010, driven by increasing demand. District heating now accounts for nearly 4% of worldwide CO_2 emissions [18]. The DH market was valued at $197.5 billion in 2024 and expected to reach $267.7 billion by 2030, reflecting a CAGR of 5.3% [21]. *Figure 5* shows the annual global energy supplies to DH networks in the context of net zero scenario by 2050 that demands much greater actions to quickly enhance the energy efficiency of current networks and transition them to renewable heat sources. *Figure 6* shows CO_2 emissions intensity index for DH production by country and region which is a measure used to evaluate how much carbon dioxide (CO_2) is emitted per unit of economic activity, energy produced, or other output.

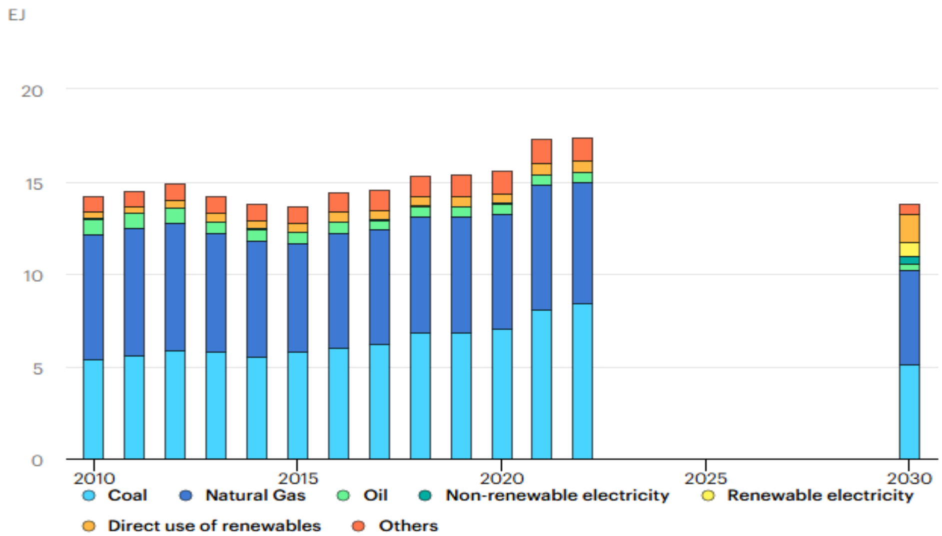

Figure 5. Annual global energy supplies to DH networks in the Net Zero Scenario [18]

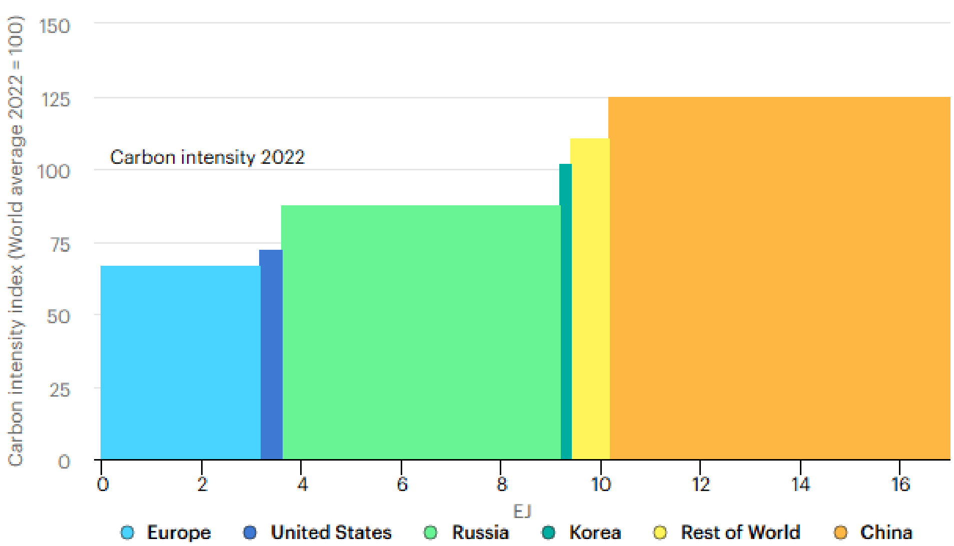

Figure 6. Carbon dioxide emissions intensity index for DH production by country and region [18]

On the other hand, District cooling increasingly impacts global energy systems, yet it carries considerable environmental consequences. Cooling currently represents roughly

20% of worldwide electricity usage, positioning it as a significant factor in emissions linked to energy [22]. Global energy needs for cooling are expected to increase from 7 EJ in 2016 to 12 EJ by 2050, representing a 45% rise [19] (*Figure 7*). If current trends persist, emissions from cooling may increase from 4.8 to 7.2 billion tons of CO_2 emitted by 2050 [22] (*Figure 8*). However, DC systems could lower CO_2 emissions by as much as 50% relative to traditional cooling methods (usually between 50–150 gCO_2/kWh) when supplied by electricity grids powered by renewables [23]. The DC market was valued at $26.79 billion in 2024 and expected to reach $48.18 billion by 2032, reflecting a CAGR of 7.87% [24].

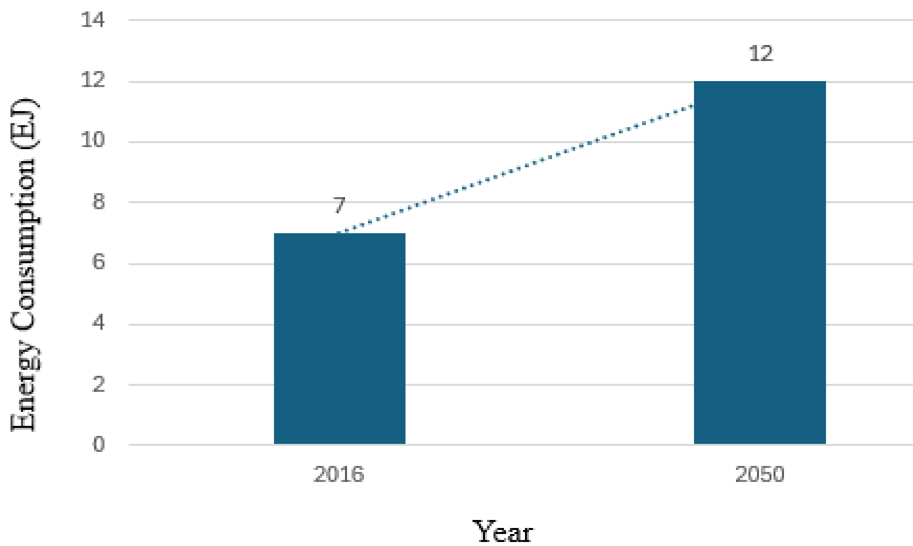

Figure 7. Estimated global increase in energy consumption of cooling systems

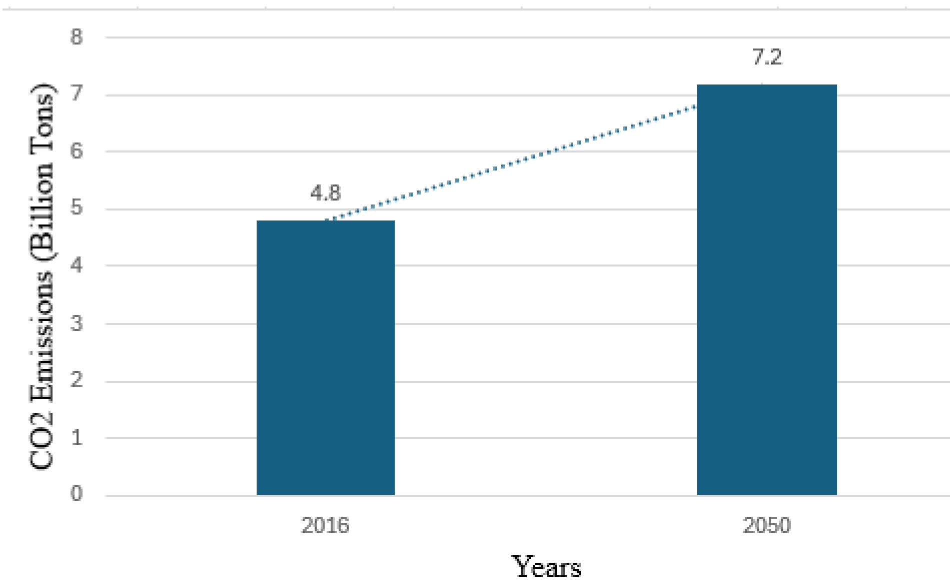

Figure 8. Estimated global increase in CO2 emissions emitted by cooling systems

1.3.3 Desalination

Desalination is the method of extracting salts, and additional compounds, from seawater or brackish water to generate drinkable water. Around the world, there are roughly 21,000 desalination facilities currently functioning, generating about 110 million m^3/day of desalinated water [25]. The biggest installations are in Saudi Arabia and the UAE, with increasing acceptance in the U.S., India, and China. Desalination is done through thermal technology (MED, MSF) or membrane technology (RO) *(Figure 9)*. RO technology was first used for brackish water desalination. The latter indeed requires less electrical energy compared to seawater since it has a lower osmotic pressure [26]. The increase in membrane lifetimes and the development of energy recovery devices to lower the energy needs for the process led to significant progress in reverse osmosis. Desalination capacity has recently grown significantly, rising from 35 million m^3/day in 2005 to 115 million m^3/day in 2020 [26].

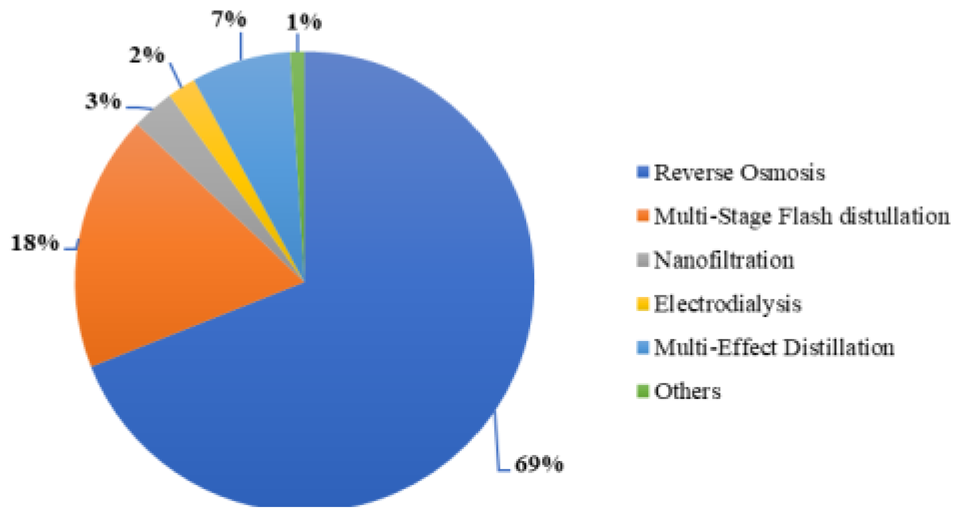

Figure 9. Worldwide current contribution of installed desalination technologies in 2020 [26]

Desalination facilities typically consume significant amounts of electricity, although it can vary based on the technologies used. Thermal desalination methods require over 5 kWh of energy for every m^3 of desalinated water generated, while RO can produce 1 m^3 of desalinated water using an average of 2.5 to 3 kWh [27]. RO emits approximately 1.7 to 2.8 kg of CO_2 per m^3 of water produced, whereas the thermal technologies MED and MSF emit 7 to 17.6 kg of CO_2/m^3 and 15.6 to 25 kg of CO_2 per m^3 of desalinated water respectively [28].

The global energy requirements for desalination in 2023 was around 2000 PJ which is equal to 2000×10^{15}J and may increase considerably by 2030, exceeding 4000 PJ (4000×10^{15}J) (≈1,111 TWh), primarily influenced by the Middle East and Africa [29] *(Figure 10)*. The yearly CO^2 emissions linked to water desalination plants currently installed and operational around the globe are estimated to be approximately 76 Mt [30] with projection reporting increases up to approximately 218 Mt by 2040, if no containment measures are taken [30] *(Figure 11)*. In 2024, the worldwide desalination market was estimated at $15 billion and is expected to grow to $29 billion by 2033, with a CAGR of approximately 7.9% from 2025 to 2033, where Middle East and Africa share the largest share estimated over 50% [31].

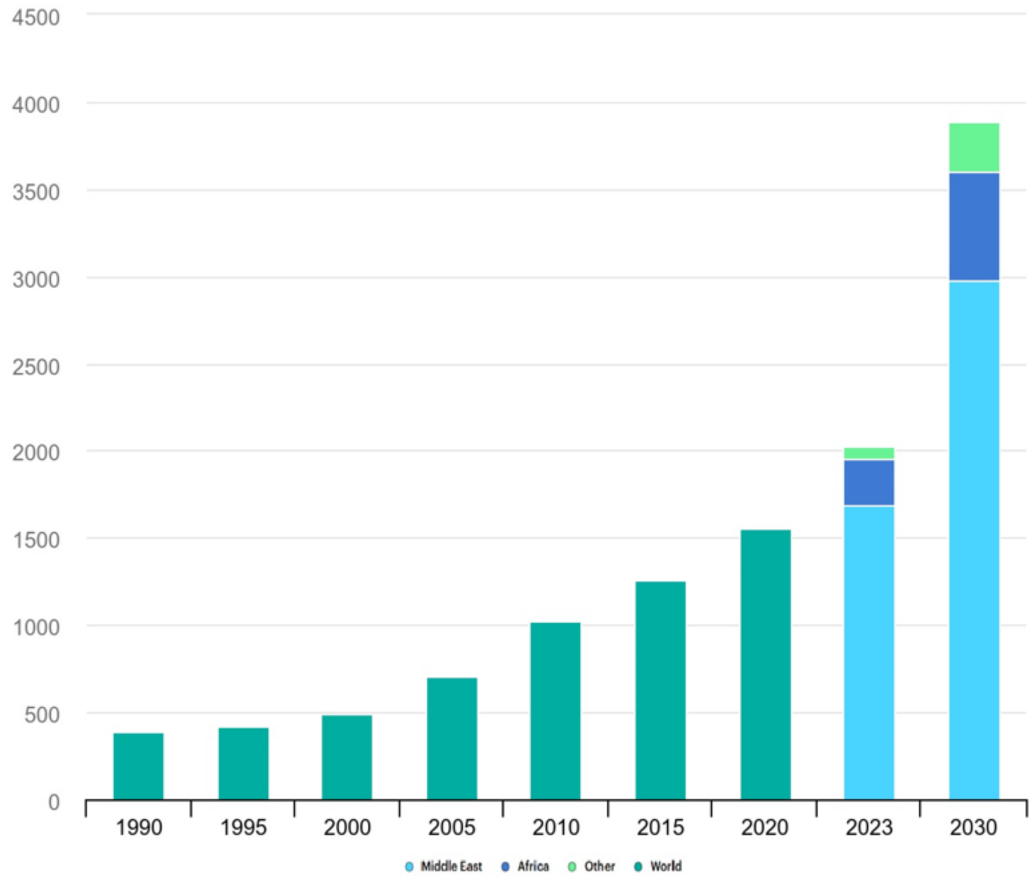

Figure 10. The propagation of global energy demand in PJ of desalination plants [29]

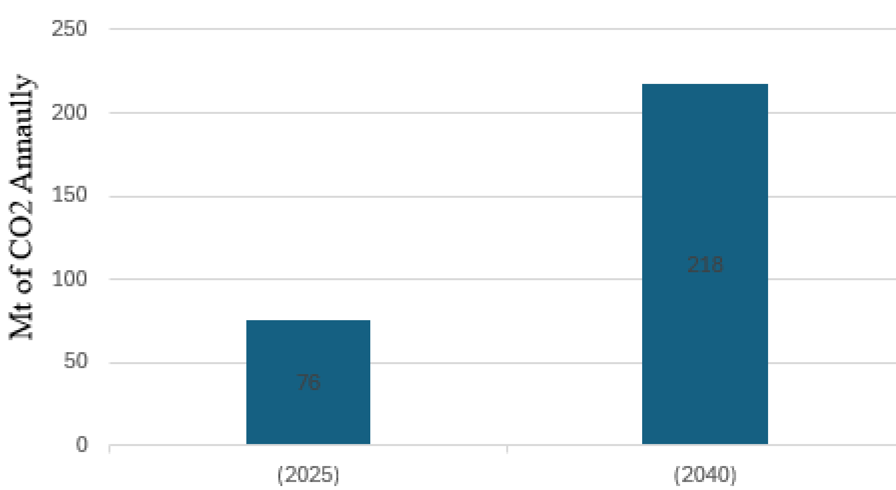

Figure 11. The estimated global annual CO2 emission from Desalination Plants [30]

1.3.4 Desalination Technologies Integration with Data Center Infrastructure

Desalination is frequently utilized in data centers to guarantee a sustainable and dependable water source for cooling systems, especially in coastal or water-limited areas. The desalinated water mainly serves as make-up water in cooling towers, where evaporation is the primary method for heat dissipation; as water evaporates, fresh water needs to be consistently supplied to keep the system functioning. The incorporation of RO systems enables facilities to recycle cooling tower blowdown water, greatly decreasing freshwater use while preserving water quality standards.

Innovative methods go beyond traditional systems to enhance sustainability by combining desalination with the waste heat produced by servers, which can be utilized to power thermally assisted techniques like Membrane Distillation (MD). These systems utilize low-grade heat that would normally be wasted, thus enhancing overall energy efficiency and decreasing greenhouse gas emissions (Waste heat-driven desalination systems) [32]. Recent studies and policy debates emphasize that data centers are emerging as major water users worldwide, elevating the need to incorporate advanced water treatment and desalination technologies into their architecture for lasting environmental sustainability [33].

1.4 Definition of Synergistic Industrial Clusters

A synergistic industrial cluster, or eco-industrial park, brings together various industries to exchange energy, heat, water, and byproducts, transforming the outputs of one facility into the inputs for another, an approach referred to as industrial symbiosis. Geothermal energy is ideally matched for these clusters as it delivers consistent, reliable heat and power that can be utilized in a tiered manner from high to low temperature applications, enhancing overall efficiency and cost-effectiveness while reducing emissions and fuel hazards.

1.4.1 Design Principles for Industrial Geothermal-Anchored Clusters

The design of industrial clusters anchored by geothermal energy is directed by principles that enhance energy efficiency, economic feasibility, and environmental advantages *(Figure 12)*. Cascading temperature utilization is essential: high-enthalpy steam from geothermal systems should be directed to energy-intensive activities, while medium-temperature heat can be utilized in less energy intensive industries, with low-temperature heat allocated for district heating or cooling. This method guarantees maximum exergy throughout the cluster [34]. Secondly, common infrastructures such as pipelines, heat exchangers, brine management systems, and CO_2 handling lowers capital and operational expenses while facilitating smooth energy distribution across various industries [35]. Third, byproduct valorization boosts sustainability and profitability by extracting minerals like silica, sodium, potassium, calcium, and lithium from geothermal brines and employing CO_2 for greenhouse enrichment or direct air capture projects [36]. Fourth, the integration of flexible technologies, including high-temperature heat pumps and heat-powered cooling systems, broadens industrial uses and enhances adaptability to fluctuating thermal requirements [37]. Ultimately, policy and permitting structures are vital in speeding up cluster development by simplifying approvals, providing financial incentives, and reducing investment risks as highlighted by IEA and NREL reports [8].

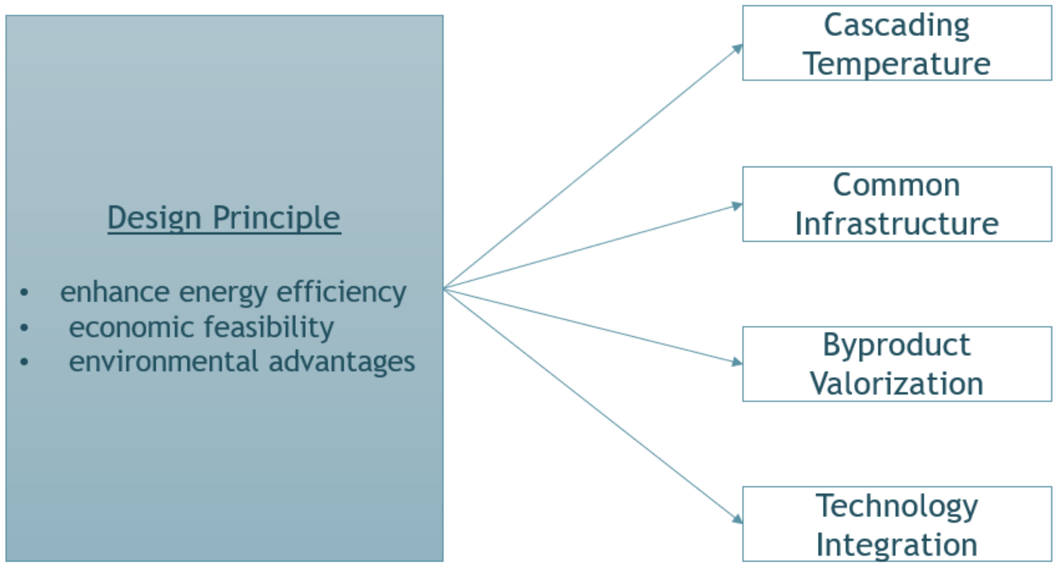

Figure 12. The basic design principle of industrial cluster

1.5 Industrial Hubs

Industrial zones are geographically concentrated regions of manufacturing and economic engagement aimed at promoting industrial growth, technological progress, and local development. They comprise industrial parks, special economic zones (SEZs), export-processing zones, and technology parks, functioning as vital catalysts for structural transformation in both developed and emerging economies. Globally, over 6,000 industrial hubs are present in 147 nations, with a notable focus in Asia resulting from export-driven growth tactics and favorable regulatory conditions [38]. In this context, incorporating geothermal energy into industrial centers signifies a growing yet still insufficiently examined opportunity mostly because of remoteness of geothermal systems. Geothermal resources offer a reliable, low-carbon supply of heat and electricity, aiding industrial operations and promoting energy efficiency via cascading utilization and collective thermal systems. Additionally, geothermal resources can serve as a unifying element for the establishment of new industrial centers, drawing energy-dependent sectors that gain from consistent and affordable thermal energy. This emphasizes a robust connection between geothermal energy, industrial centers, and infrastructure, where energy resources affect industrial placement, industrial needs spur infrastructure advancement, and infrastructure subsequently improves the technical and economic viability of geothermal utilization.

1.5.1 Importance of Industrial Hubs

Industrial hubs significantly contribute to economic development by drawing foreign direct investment (FDI), enhancing exports, and creating job opportunities. They generate agglomeration economies, allowing companies to gain from closeness to suppliers, skilled workforce, and common infrastructure, which lowers costs and improves efficiency [38]. Additionally, these hubs promote innovation and competitiveness by facilitating knowledge exchange and technological progress, allowing companies to succeed in global markets [39]. In addition to economic advantages, industrial centers enhance regional growth by promoting urbanization, upgrading infrastructure, and elevating living conditions in nearby regions. *Table 2* shows the importance of industrial hubs on several basis.

Table 2. The importance of industrial hubs on several basis

Economic Development
Agglomerated Economies
Promote Innovation
Enhance Regional Growth

1.5.2 Importance of Industrial Infrastructure in Hubs

Industrial centers rely on various essential types of infrastructure that directly affect productivity, competitiveness, and sustainable growth. Transport infrastructure, such as pipelines, highways, rail systems, ports, and airports, is vital as it facilitates the smooth transport of raw materials and finished goods, lowering logistics expenses and enhancing supply-chain integration [40]. Energy infrastructure is equally vital, as dependable electricity grids and substations guarantee continuous industrial activities and avert expensive production setbacks [40]. Industrial centers depend on water provision and waste-management infrastructures, which guarantee consistent access to processing water and adherence to environmental regulations, an ever more crucial element in sustainable industrial progress [40]. As modern manufacturing advances, digital infrastructure like broadband networks, data centers, and communication systems has become essential for automation, real-time monitoring, and involvement in global value chains [41]. Ultimately, robust social infrastructure— encompassing housing, healthcare, and workforce training facilities bolsters labor stability and improves worker productivity, thereby increasing the competitiveness and resilience of industrial centers [42]. *Table 3* shows the types, benefits, and components of industrial Infrastructure.

Table 3. The types, benefits, and components of industrial Infrastructure

Infrastructure Type	Key Function	Components
Transportation	Efficient movement of sources and products	Pipelines, Ports, Highways, Railways
Energy	Reliable Power Uninterrupted Operations	Electricity Grids, Substations
Water and Waste	Stable Water Supply Environmental Compliance	Water Treatment, Waste management
Digital	Automation Real-Time Monitoring	Data Centers, Communication Systems
Social	Labor Stability enhanced Productivity	Housing, Healthcare, Training Centers

Chapter 2: Geothermal Potential Integration in Italy

Italy possesses a long history in geothermal energy and continues to be a world leader in this area. In 1904, Italy became the first in the world to generate electricity using geothermal energy. More than a hundred years later, Italy ranked among the top producer of geothermal energy globally [43].

2.1 Geothermal Resource Potential

Geological research suggests that Italy has a vast geothermal resource base compared to its existing utilization. A report from the Italian Geothermal Union approximated that the recoverable onshore geothermal energy (to a depth of 5 km) varies between ~500 million to 10 billion tons of oil equivalent (Mtoe) – equating to (5 – 104) × 10^2 EJ, or about 3 to 60 times Italy's yearly primary energy use [44]. One evaluation indicates that Italy might realistically establish as much as 13 GW of geothermal electric capacity, generating 115 TWh annually (nearly 20 times the existing production) [45]. This encompasses high-enthalpy regions appropriate for power generation, and medium-enthalpy sources that would fit for direct heating applications or binary-cycle facilities. Undoubtedly, the geothermal potential greatly surpasses current utilization, presenting a significant opportunity for Italy's energy transition if effectively tapped.

2.1.1 Geothermal Potential Zones

Italy lies in a geologically active region with a relatively thin crust and high heat flow mostly occurring in the western sector. Mapping studies have divided the Italian territory into four major geothermal categories [46] (*Figure 13*):

1. Category A: encompasses areas where at least one aquifer that contains fluids at temperatures higher than 150° C within depth of 3 km occur [46]. All those areas are in the major belt of a hydrothermal anomaly which runs from NW-SE direction from Genova to the Aeolian archipelago, astride the Tyrrhenian border of the peninsula [46]. This belt contains all the high temperatures geothermal fields

identified so far (e.g., Larderello, Mt. Amiata). Moreover, areas of category A can also be found in southern Sardinia (central part of the Campidano graben) and at the Pantelleria island (in Sicily Channel) [46].

2. Category B: comprises areas that contain at least one aquifer that with fluid at temperatures between 90° and 150° C at depth of 3 km [46]. Areas of these category are usually located at the boundaries of category A areas, but they are also identified in small, isolated parts of mainland Italy and the islands, such as the inner foothills of the Alpine chain, the northern and southern borders of the lower Po valley, the margins of the Bradano trough, and in Sicily and Sardinia [46]. All areas of this category must be considered of moderate geothermal interest.
3. Category C: these areas contain at least one aquifer at temperatures between 39° and 90°C within the depth of 3 km [46]. Areas of this category are mainly located in correlation to the central part of the Alpine and Apennine mountain ranges. It also contains the entire region of Apulia, most of Calabria, and a significant part of Sicily (the Hyblean region, the northern mountains ranges, and the western region), the whole eastern part and the north-western tip of Sardinia [46]. These areas can be considered as low enthalpy geothermal potential.
4. Category D: Are areas that don't have any major regional aquifer within the depth of 3 km, but the temperatures can reach any value [46]. This category is divided into four sectors: 1) The entire Po Valley, from the bottom of the pre-Alpine arc to the bottom of the northern Apennines, 2) The belt of foothills and coastal plain east of the Central Apennines, 3) The central part of the Bradano trough in southern Italy, and 4) the Caltanissetta trough in central Sicily [46]. These areas have very low geothermal potential.

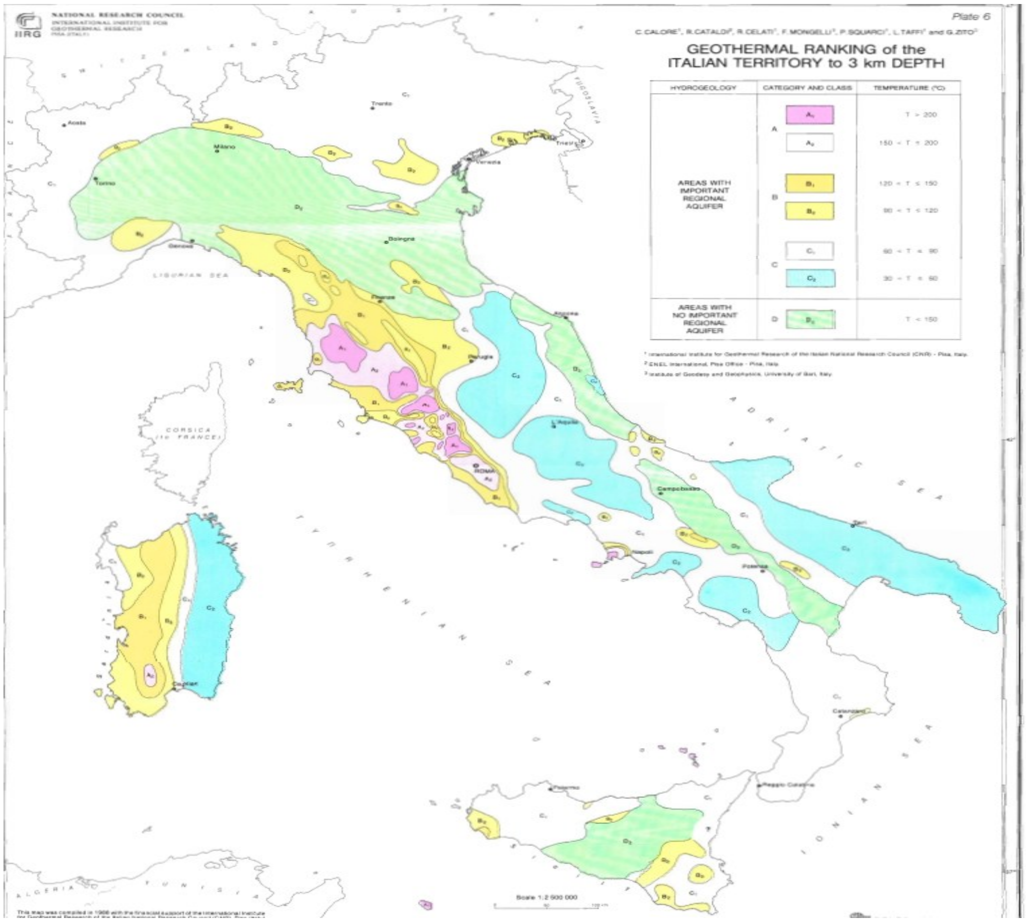

Figure 13. Map of the Italian geothermal areas to 3 km depth, divided by their ranking [46]

2.1.2 Major Operating Geothermal Fields

1. *Larderello Geothermal Complex*

The Larderello Geothermal Complex, found in Tuscany, Italy, is regarded as the origin of contemporary geothermal energy. It gained historical importance in 1904 when Piero Ginori Conti effectively produced electricity through geothermal steam, marking the first instance this was accomplished globally. By 1913, Larderello was home to the initial commercial geothermal power facility, and it still stands as one of the largest and most sophisticated geothermal fields in the world, acting as a standard for sustainable energy generation.

- Capacity and Structure: Larderello Geothermal Complex consists of more than 500 geothermal wells divided between production and re-injection well for the sustainability of the system [47]. The area includes 34 power stations and 37 generating units, located within a small region close to Larderello, Pomarance, and Montecerboli. The overall installed electric capacity is around 800 MW, featuring the prominent "Valle Secolo" complex which by itself provides nearly 120 MW through two 60 MW condensing steam turbines [48].

- Resource classification and Geology: The Larderello Geothermal Complex is one of the fewest systems to be characterized as vapor dominated, high enthalpy system yielding superheated steam that is directly exploited for electricity generation [49]. It exists in a Miocene–Pliocene back-arc extensional setting of the northern Apennines, generated by slab rollback and crustal thinning to approximately 20–22 km, which resulted in fault-controlled permeability and raised pull-apart basins [50]. The heat source consists of a shallow granite intrusion located at depths of 4–9 km and a more extensive mantle-rooted hot body (~32,000 km^3) [51], creating a local heat flow anomaly of ~1000 mW/m^2 in contrast to the regional 100–200 mW/m^2 [52].
- Reservoir system and Management: The reservoir exhibits stratification: an impermeable layer rests above an upper carbonate–anhydrite section at approximately 1 km depth (220–250 °C, ~20 bar) and a deeper metamorphic base at around 3 km (300–350 °C, ~70 bar), featuring fractured metamorphic rocks and granitic intrusions at even deeper levels [53]. To maintain reservoir pressure and fluid balance, some drilled wells were dedicated to reinjection. This approach enhanced the production wells' flowing pressure, compensating for the loss due to extraction [54].

The electricity production process at the Larderello Geothermal Complex starts with superheated steam taken from deep geothermal wells. The steam initially goes into a separator, where liquid water is extracted and directed back into the reservoir to uphold pressure and sustainability. The isolated steam subsequently moves to a turbine, where its heat energy is transformed into mechanical energy, powering a generator to generate electricity. Non-condensable gases in the steam are removed by a gas extractor and cooled in a gas cooler to avoid efficiency decline and corrosion. Once it exits the turbine, the steam is reverted to water in a condenser, utilizing cooling supplied by a cooling tower. The chilled water is subsequently reintroduced into the geothermal reservoir, finalizing a closed-loop system that guarantees ongoing electricity production while maintaining the geothermal resource (*Figure 14*).

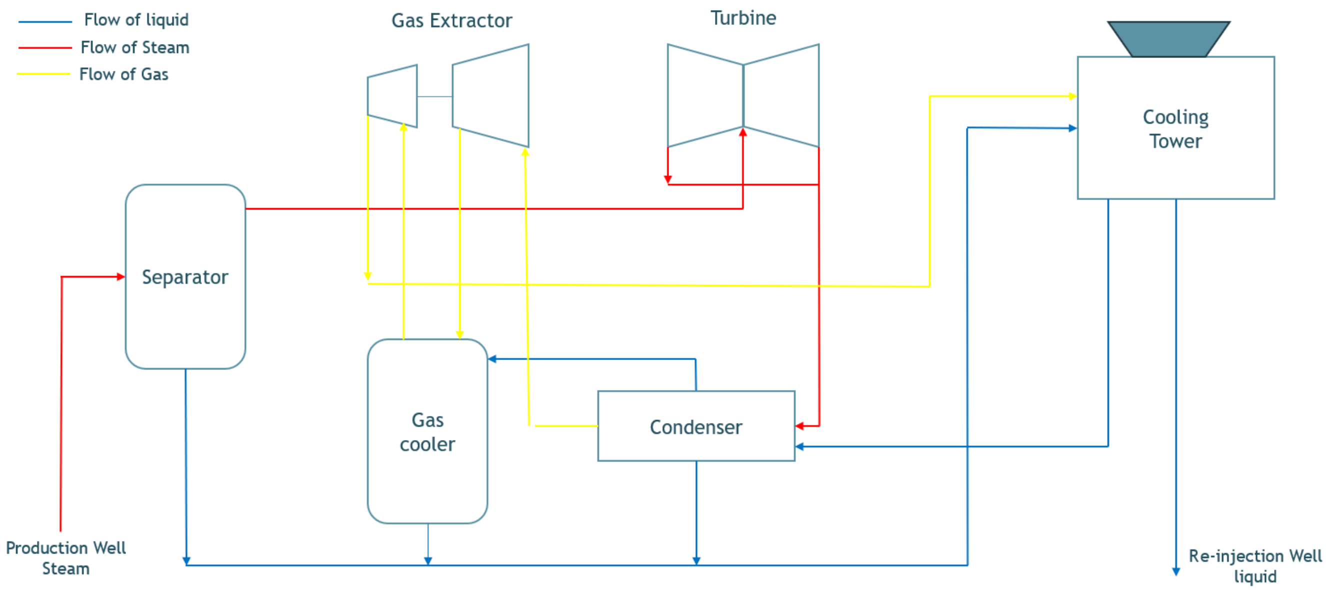

Figure 14. Sketch of the electricity generation process at the Larderello geothermal power plants.

2. *Ferrara Geothermal Complex*

The geothermal complex in Ferrara in the heart of Emilia Romagna Region, situated close to Casaglia southeast of Ferrara, ranks among Italy's most important medium-enthalpy geothermal district heating systems. It was developed after the identification of a hot-water reservoir during AGIP's hydrocarbon explorations in the late 1950s and started functioning in 1990 as a component of Ferrara's unified heating network.

- Capacity and Structure: It utilizes two production wells, extracting pressurized hot water from depths of 1,100 meters (Casaglia 1 well) and 1,960 meters (Casaglia 20 well) [55]. This extraction method minimizes energy usage and reduces production and consumption costs. The geothermal segment delivers approximately 14 MW of thermal energy and generates around 75,000 MWh each year [55]. The district heating system covers 160 km and serves 25,000 housing units (geothermal energy accounts for 43% of the system's energy supply) [55].

- Resource Classification and Geology: The Ferrara geothermal resource is identified as a medium-enthalpy hydrothermal system, exhibiting water temperatures, which is better suited for district heating instead of electricity production [56]. The reservoir is geologically situated within Mesozoic carbonate formations like Dolomia Principale and Calcari Grigi, found under the Po Plain inside the Ferrara Folded Arc, a structural elevation created by Apennine tectonics [56]. These porous carbonate formations facilitate effective heat extraction and reinjection, aided by a significant thermal gradient and convective heat movement that establishes a consistent geothermal anomaly [56].
- Reservoir System and Management: The Ferrara geothermal reservoir operates as a closed-loop-like hydrothermal system, where two production wells extract water and reinject cooled water to maintain pressure and sustainability [56]. Management involves ongoing observation of temperature, pressure, and chemical makeup to avoid scaling and guarantee sustainability over time [56].

Hot water is drawn from a medium-enthalpy geothermal reservoir via two production wells. This water, at roughly 100 °C, is brought to the surface and sent to heat exchangers, where its thermal energy is conveyed to the district heating system without mixing with the network water [56] (*Figure 15*). Following heat exchange, the cooled geothermal water (approximately 85 °C) is reintroduced into the reservoir via reinjection wells to uphold pressure and guarantee sustainability [56].

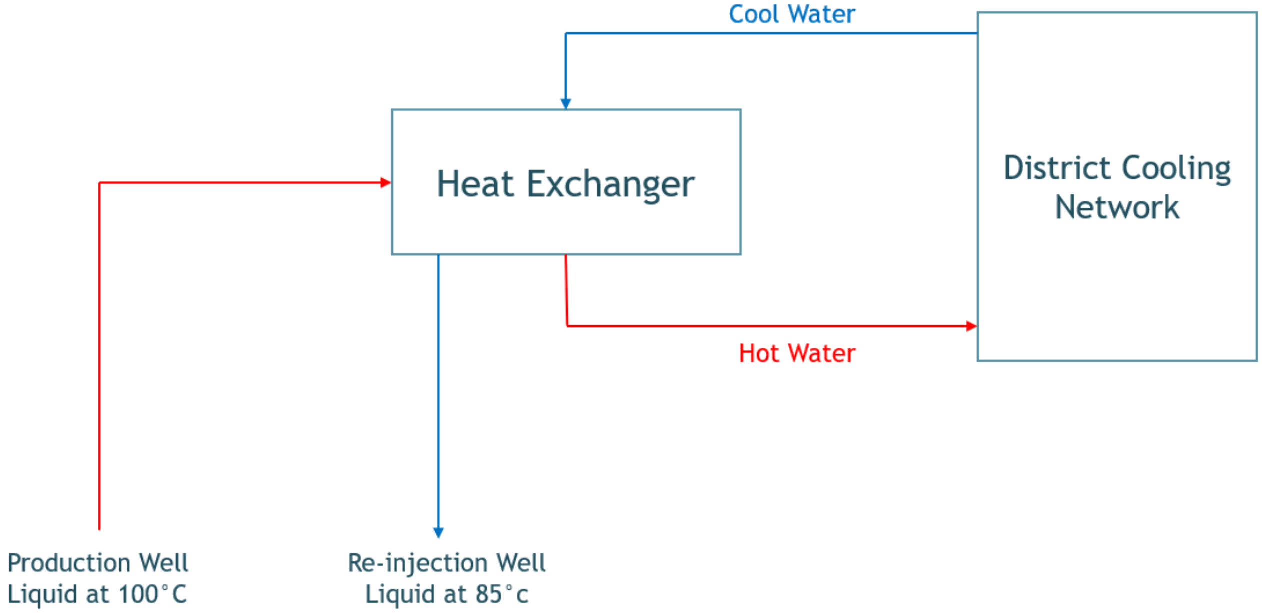

Figure 15. District heating system of the Ferrara Geothermal Complex

The following *Table 4* compares the 2 geothermal complexes in Italy, showing the difference in the high enthalpy system (Larderello) and medium enthalpy system (Ferrara), and that how each system is utilized.

Table 4. The different features between 2 types of geothermal systems Larderello and Ferrara

Feature	Larderello Geothermal Complex	Ferrara Geothermal Complex
Location	Tuscany	Emilia-Romagna Region
System Type	Vapor-dominated, high-enthalpy system	Medium-enthalpy hydrothermal system
Primary Use	Electricity generation	District heating
Installed Capacity	~800 MW (34 power stations, 37 generating units)	~14 MW thermal
Resource Temperature	Upper reservoir: 220–250 °C; deeper reservoir: 300–350 °C	~100 °C

Depth of Wells	Upper reservoir: ~1 km; deeper reservoir: ~3 km	Casaglia 1: 1,100 m; Casaglia 20: 1,960 m
Geology	Miocene–Pliocene back-arc extensional setting; granite intrusion; mantle-rooted hot body	Mesozoic carbonate formations (Dolomia Principale, Calcari Grigi) under Po Plain
Reservoir Management	Reinjection wells maintain pressure and fluid balance	Closed-loop system: reinjection at ~85 °C after heat exchange

2.1.3 Medium Enthalpy Geothermal Potential

In Italy, medium-enthalpy resources are generally characterized by fluid temperatures around 90–150 °C (occasionally reaching ~ <150 °C) found at depths of several kilometers. Important areas for medium-enthalpy resources fall in the B category that roughly cover the 10-12 % of the Italian Territory (Figure 13) [46] and are represented by:

- The Transition zone between Alpine chain and the Po-Venetian plain
- Colli Euganei area south of Padua (Veneto Region)
- B2 Areas north of Bologna and between Venezia and Trieste
- B1and B2 areas east of Napoli, between Campobasso and Potenza
- B2 areas in western Sicily, especially B1 area of Sciacca
- B2 areas in the Hyblean Platform (south-eastern Sicily)

These are not areas of boiling steam but rather excellent hot water resources ideal for binary-cycle electricity production (ORC) and for direct thermal applications (district heating and cooling, industrial process heat, etc.). Medium-enthalpy resources are mostly unused for energy production; nonetheless, they have the potential to aid binary-cycle facilities or cogeneration systems (REF). In conclusion, Italy's focus for high-enthalpy energy continues to be on the fields of Tuscany, whereas medium-enthalpy regions offer potential for gradual production and direct heat applications – yet still need additional drilling and development.

2.2 Major Industrial Hubs and Infrastructure

The industrial areas presented in this section constitute a subset of sites potentially suitable for the exploitation of medium-enthalpy geothermal energy mentioned in the above section. Other areas may also be appropriate depending on local geological conditions, energy demand, and infrastructure availability. This selection is intended as illustrative rather than exhaustive.

1. North of Bologna: The metropolitan region is one of Italy's key manufacturing centers, showcasing a significant density of machinery, mechatronics, and notably packaging industries—commonly known as the "Packaging Valley"—dominated by global entities like IMA and GD, which jointly represent approximately 55% of local manufacturing jobs [57]. In addition to this primary sector, the region also features considerable operations in textiles, automotive parts, insurance, and agri-food production [58], while the adjacent Altedo region hosts about 110 SMEs primarily engaged in metalworking, paper, and construction-related sectors [57]. Bologna serves as a key national logistics hub where the A1 (Autostrada del Sole) and A13 motorways meet, with the A13 offering a direct route north to Padua, supported by high-speed and freight rail lines along the Naples–Milan route and the Bologna Interporto, a major European intermodal freight village with seamless road–rail connections [58]. Bologna Guglielmo Marconi Airport, the fifth-busiest airport in Italy, supports air freight and managed approximately 14000 tons of cargo in 2017 [58]. Significant industrial and logistics areas are located just north of the city, such as Prologis Park Bologna Interporto, one of the largest intermodal logistics parks in Europe featuring direct rail connectivity and A13 motorway access [58], the Altedo production center providing greenfield opportunities and

effective highway access for companies aiming to bypass urban traffic [58], along with other key clusters like Centergross and the industrial sectors of Casalecchio.

Medium-enthalpy geothermal energy has the potential to deliver process heat for packaging, metal fabrication, and textile manufacturing, in addition to space heating for warehouses and logistics centers. In the agri-food industry, it may assist in drying, pasteurization, or various low-to-medium temperature procedures, while in manufacturing machinery and automotive components, it could provide heat for washing, preheating, or various thermal treatments—contributing to lower fossil fuel consumption and operational expenses in the industrial areas north of Bologna.

2. Veneto Region: The Veneto region features a polycentric industrial system backed by key centers and advanced transport infrastructure. One of the key industrial hubs is the Padua region, where the Zona Industriale di Padova (ZIP) stands as one of the largest industrial areas in northeastern Italy, accommodating more than 1,500 firms and incorporating a significant intermodal logistics platform connected to national and European freight systems. Another crucial center is Venice, especially the industrial-port complex of Porto Marghera, an extensive zone covering over 2,000 hectares that integrates heavy industry, petrochemicals, and port logistics, featuring extensive road, rail, and canal infrastructure. In a broader sense, Veneto's industrial framework is bolstered by a substantial number of small and medium-sized businesses spread throughout provinces like Treviso, Vicenza, and Verona, focusing on industries such as textiles, machinery, and agri-food production [60]. In general, the competitiveness of the region depends on the integration of industrial clusters, intermodal logistics hubs, ports, and transportation routes, creating one of the most efficient production and distribution networks in Italy.

Medium-enthalpy geothermal energy has the potential to provide sustainable process heat for the region's heavy industry, petrochemicals, textiles, machinery, and agri-food sectors. In industrial areas such as Porto Marghera and the Zona Industriale di Padova, it may assist with drying, washing, pasteurization, and preheating processes, in addition to space heating for storage and office buildings.

3. <u>The eastern plain of Naples</u>: Covering the Nola–Acerra–Pomigliano d'Arco region, stands as one of southern Italy's key industrial and logistics pathways, emphasizing automotive production, waste-to-energy, chemicals, and extensive distribution. An important anchor is the Stellantis N.V. Ltd. factory in Pomigliano d'Arco, which has approximately 6,000 employees and manufactures Alfa Romeo and Fiat cars [61], while the nearby Acerra features a significant waste-to-energy plant with a capacity of roughly 120 MW along with a chemical industrial facility. Logistics is crucial at the Interporto Campano in Nola, a vast distribution hub hosting around 150 businesses and exceeding 462,500 m^2 of storage area, enhanced by food-processing and pharmaceutical operations throughout the region [62]. Connectivity is remarkable, since the region is positioned at the crossroads of the A1, A16 (Naples–Bari), A30 (Caserta–Salerno), and A3 highways, is accessible through the high-speed [62]. Napoli Afragola railway station—established in 2017 and connecting northern and southern Italy with 36 daily high-speed trains—and enjoys closeness to Naples Capodichino Airport and the Port of Naples, with logistics augmented by the Naples dry port located in Nola [63]. From the standpoint of industrial policy, the CIS Interporto Campano constitutes a key logistics and industrial area that has been part of Campania's Special Economic Zone since 2017 and, starting January 2024, within the national ZES Unica, offering tax and customs advantages [62], while nearby locations like the ASI industrial zone of Acerra and the Naples–Afragola industrial district are bolstered by national PNRR investments

and financial support from European SEZ initiatives focused on enhancing rail and logistics facilities.

Medium-enthalpy geothermal energy has the potential to deliver sustainable process heat for automotive manufacturing at Stellantis, chemical production in Acerra, and waste-to-energy operations, along with food-processing and pharmaceutical facilities in logistics centers like Interporto Campano. It may also provide heating for storage facilities, workplaces, and manufacturing sites, enhancing operational efficiency while decreasing dependence on fossil fuels. Incorporating geothermal energy into this compact industrial and logistics area would improve energy sustainability and reduce expenses across various high-demand industries.

4. Western Sicily: Which includes the provinces of Palermo, Trapani, and Agrigento, relies mainly on tourism, agriculture, and fisheries for its economy, instead of heavy industry. Olive groves, vineyards—especially those crafting Marsala wine—and citrus farming prevail in inland regions, whereas the Trapani–Marsala salt pans symbolize a historic and ongoing salt-producing area intricately linked to local wine production. Palermo serves as the regional capital and acts as Sicily's primary center for industry and commerce, with a focus on services, trade, food processing, and some light manufacturing, including food items and machinery [64]. Transport infrastructure facilitates these functions via prominent ports, such as the Port of Palermo for both commercial and cruise activities, Port of Trapani for ferry services, and the fishing port of Mazara del Vallo; air connections are offered by Palermo Falcone e Borsellino Airport, Trapani Birgi Airport, and the newer Comiso Airport, primarily catering to low-cost airlines [65]. The area is traversed by important road corridors like the A29 (Palermo–Mazara del Vallo) and the A19 (Palermo–Catania), along with rail connections on the Palermo–Trapani/Mazara

and Palermo–Catania routes. Western Sicily is part of the Zona Economica Speciale Sicilia Occidentale from an industrial policy viewpoint, focusing on agribusiness, fisheries, and logistics, encompassing major ports like Palermo, Termini Imerese, and Mazara del Vallo, while Palermo's industrial areas (such as Brancaccio and Valenzano) and the old Fiat facility in Termini Imerese are undergoing redevelopment, with a growing focus on renewable energy and sustainability initiatives [66].

Medium-enthalpy geothermal energy could benefit agribusiness, food processing, and light manufacturing in Western Sicily by supplying heat for drying, pasteurization, and various low- to medium-temperature operations. It might also provide space heating for industrial buildings, storage facilities, and offices, while aiding sustainability efforts in redeveloped areas such as the former Fiat site in Termini Imerese.

5. Southeastern Sicily: Covering the provinces of Siracusa and Ragusa, combines heavy industry with strong agricultural and tourism activities, creating a diversified regional economy. The Siracusa–Gela industrial corridor hosts Italy's largest oil refinery and major petrochemical complexes, while nearby Augusta functions as a key energy hub with oil terminals and energy-related firms [67]. Alongside heavy industry, the provinces of Ragusa and Siracusa are important agricultural producers, specializing in citrus fruits, nuts, table grapes, and viticulture, while tourism has expanded rapidly thanks to UNESCO-listed Baroque cities such as Ragusa Ibla, Noto, and Scicli. Light manufacturing, including food processing and aerospace components, is also present, particularly in the broader Catania–Siracusa area. Transport infrastructure supports this industrial mix through the Port of Augusta and Port of Siracusa, which handle oil and petrochemical traffic, as well as the passenger ferry port at Pozzallo with links to Malta; air connectivity is ensured by

Catania Fontanarossa Airport and Comiso Airport [67]. Road and rail links are provided by the A18 (Messina–Siracusa) and A19 corridors and by rail lines connecting Messina–Siracusa and Catania–Siracusa. From a policy and planning perspective, the area falls within the Zona Economica Speciale Sicilia Orientale, which focuses on energy, logistics, and high-tech industries, encompassing industrial parks such as Priolo Gargallo for petrochemicals and engineering and the Etna Valley, which promotes advanced manufacturing, biotechnology, and ICT [67].

Medium-enthalpy geothermal energy may supply process heat for petrochemical and oil refining activities in the Siracusa–Gela corridor, along with food processing, viticulture, and light manufacturing operations in Ragusa and Siracusa. It could additionally provide space heating for industrial sites, storage facilities, and offices, aiding the region's varied industrial and agricultural industries. Integrating geothermal energy in Southeastern Sicily may decrease fossil fuel use, cut operational expenses, and promote the sustainability of its energy-heavy industries and tourism-related facilities.

6. Sciacca: Is a small seaside region located in the Province of Agrigento, where the economy primarily relies on agriculture, fishing, and seasonal tourism instead of heavy industry [68]. The nearby landscape features olive plantations, vineyards that yield local wines, citrus orchards, and vegetable farms, while the Port of Sciacca—boasting approximately 600 berths—is vital for providing shellfish and bolstering small-scale seafood processing operations. Tourism serves as a significant revenue stream, especially in the summer, as the town draws tourists for its beaches, classic Carnival, and the historic Terme di Sciacca. Economic activity is additionally bolstered by small workshops in food processing and textiles that mainly cater to local needs. From a transportation standpoint, Sciacca is quite remote, without direct motorway or rail links; it is primarily accessed by the SS115 regional road

connecting Agrigento and Marsala, and the local railway station has been out of service since the 1970s, thus making road transport the sole terrestrial alternative. Palermo Falcone e Borsellino Airport (around 90 km away) and Trapani Birgi Airport (approximately 110 km) offer air access, while the small Class III port of Sciacca, which has two piers, is being modernized to enhance local maritime services [69].

In Sciacca, medium-enthalpy geothermal energy might facilitate small-scale food processing, as well as wine and olive oil production, alongside greenhouse farming by offering low- to medium-temperature heat for drying, pasteurization, and warming the soil. It may also provide space heating for workshops, tourism establishments, and nearby thermal baths, like the Terme di Sciacca, boosting both industrial and tourism-related endeavors. Utilizing geothermal energy in this seasonal, small-scale economy may decrease dependence on fossil fuels, enhance energy efficiency, and encourage sustainable development in the local area.

2.3 Data Centers and Computing Infrastructure

The data center industry in Italy has expanded swiftly in recent years, turning into a vital framework for the nation's digital economy. By 2024, Italy has 168 functioning data centers with a total installed IT capacity of approximately 513 MW, reflecting a 17% rise compared to 2023 [70]. These facilities cover more than 333,000 m² of floor area [70]. The growth of industry ranks among the quickest in Europe, fueled by increasing demand for cloud services, business digitization, and emerging technologies. Forecasts suggest that the trend will persist – Italy’s installed capacity (approximately 300 MW in 2023) is anticipated to increase by around 30% per year, attaining 1–1.5 GW by 2030 [71]. This expansion is drawing considerable foreign investment and placing demands on energy infrastructure to match the increasing demand.

2.3.1 Geographical Distribution of Data Centers

Data centers in Italy are focused on several major markets, mostly distributed in Northern Italy (Figure 16). Lombardy (the Milan area) serves as the main center, accounting for nearly 60% of the nation's capacity (approximately 318 MW) [70]. Milan represents about 46% (≈238 MW) of Italy’s total capacity, positioning it as the leading location and cloud cluster, surpassing other Southern European capitals such as Madrid (172 MW) [70]. This is because Milan serves as Italy’s economic and connectivity hub: it features a dense network of exchanges (e.g., the Milan Internet Exchange), closeness to major corporate headquarters, and acts as a gateway connecting Europe to Mediterranean and Asian subsea cables. Other significant markets consist of Rome (the second-largest center), Veneto, Bologna, and Emilia Romagna regions, each having a few facilities. Industry surveys indicate that Milan possesses most of the current capacity and 98% of future capacity in development, highlighting its ongoing significance [72].

Figure 16. Italian data center geographical distribution. Data related to 2025 [73]

An important aspect of choosing locations for new data center projects is the accessibility and mapping of data transmission and power resources on both national and international scales. In Italy, the Federated National Infrastructure Information System (SINFI) acts as the main digital registry for physical infrastructure, offering georeferenced information on telecommunication networks (such as fiber optic), electric power grids, and various utility infrastructures, whether aboveground or underground, to aid in territorial planning and infrastructure investment [74].

From the viewpoint of digital connectivity, having high-capacity fiber optic cables – whether on land or underwater – is crucial for extremely fast connections, minimal latency, and global data transfer [74]. Specifically, Sicily and various southern areas act as crucial landing sites for submarine cables that link Europe to North Africa, the Middle East, and the Eastern Mediterranean. Examples consist of networks such as GO-1 Mediterranean and MedNautilus, along with new high-capacity backbones like Unitirreno, connecting Mazara del Vallo to Genoa and other national centers, establishing Italy as an essential digital hub in the Mediterranean region [74].

On the electricity front, linking the national grid via high-voltage networks and underwater cables—like the Tyrrhenian Link project joining Sicily, Sardinia, and the mainland—enhances the capacity and robustness of electricity transmission, essential for delivering high availability and energy demands to data centers [74].

2.3.2 Energy Consumption of Data Centers

Data centers require a significant amount of energy—Italy's facilities used around **7 TWh** in 2024 and are projected to reach **10 TWh** by 2027 and **20 TWh** by 2030 (roughly 6% of Italy’s current electricity demand) [75] (Figure 17). To reduce environmental effects, operators are making significant investments in renewable energy. Approximately 80% of the electricity used by data centers in Italy is believed to originate from renewable sources (either directly or through contracts) [71]. This is enabled by Italy's national energy mix (approximately 46% renewable generation) and by direct efforts from operators: many have pledged to supply facilities entirely with green energy.

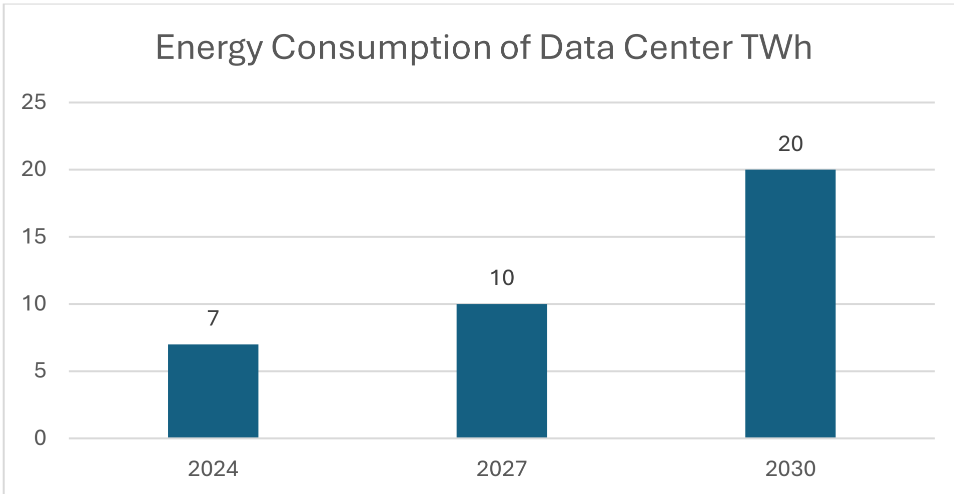

Figure 17. Expected increase of energy consumption of data centers in Italy

2.3.3 Environmental Impact of Data Centers

The carbon intensity of the Italian national grid for 2025 is 310 kg/MWh [76]. Italian data centers are projected to consume around 7,000,000 MWh of electricity based on their capacities which is estimated to increase in the upcoming years [70]. Based on this we can estimate the amount of CO_2 produced by Italian Data center using the following formula where carbon intensity measures the amount of carbon dioxide (CO_2) emitted per unit of activity. It's a key metric for understanding the environmental impact of energy, industry, or economies:

- $Amount\ of\ CO_2 = Carbon\ Intensity\frac{kg}{MWh} \times MWh\ of\ Electricity$ **[Eq.1]**

Based on this formula the amount of CO^2 emitted annually by Data centers in Italy is around 2.17 x 10^6 million tons CO2. This amount has led to an effective integration of data centers with lower emissions.

Cooling Requirement is an important factor to be considered in data centers. Chilling servers typically use significant amounts of water. Worldwide, one large data center can consume millions of liters of water daily for its cooling needs [77]. Italian facilities in warm city regions also depend on water-cooled chillers. While accurate Italian data is limited, significant cooling demands can stress local water supplies, particularly during the summer when dry and hot conditions frequently occur. This has sparked interest in cooling systems that conserve water (such as free-air, indirect evaporate systems) and in the repurposing of waste heat.

2.3.4 Power Usage Effectiveness of Data Centers

Power Usage Effectiveness (PUE) is a measure of how energy-efficient a data center is. It is determined by the ratio of the overall energy used by the whole facility (encompassing cooling, lighting, and other support systems) to the energy used by the IT devices (servers, storage, and networking). An ideal PUE is 1.0, meaning all energy goes directly to IT equipment with no overhead.

- $PUE = \frac{Total\ Facility\ Energy}{IT\ Equipment\ Energy}$ **[Eq.2]**

Data centers in Italy have consistently enhanced their PUE. Surveys indicate that the average PUE in the industry is approximately 1.48, with standard facilities falling between 1.35 and 1.60 [78]. Recent installations have been significantly more efficient: numerous cutting-edge facilities aim for a PUE of ≤1.3, with some reaching even lower [79]. Design strategies such as cold aisle containment, free cooling (utilizing outside air or groundwater for cooling), and efficient UPS and CRAC systems are now common to reduce PUE.

Chapter 3: Energy and Environmental Analysis

3.1 Organic Rankine Cycle for Electricity Production

The Organic Rankine Cycle (ORC) is a thermodynamic loop that operates in a closed system, utilizing a low-boiling organic fluid to transform heat into energy. A standard ORC system includes four primary parts: a pump, an evaporator (heater), an expander (turbine), and a condenser [80] (Figure 18). In a geothermal-ORC facility, hot geothermal fluid (e.g. brine at approximately 90 - 150 °C) transfers heat in the evaporator to vaporize the working fluid; the resulting high-pressure vapor drives the expander to produce work, then it is condensed and pumped back to the evaporator. ORC systems are commonly used to transform low-to-medium temperature geothermal heat into electricity [81]. Astolfi et al. [81] observed that low/medium enthalpy fields usually range from 120 to 180 °C, with 70–80% of geothermal resources found beneath 150 °C. Within this temperature range, ORC/binary plants excel over traditional steam cycles or other binary cycles (such as Kalina) due to their straightforward design and adaptability of working fluids.

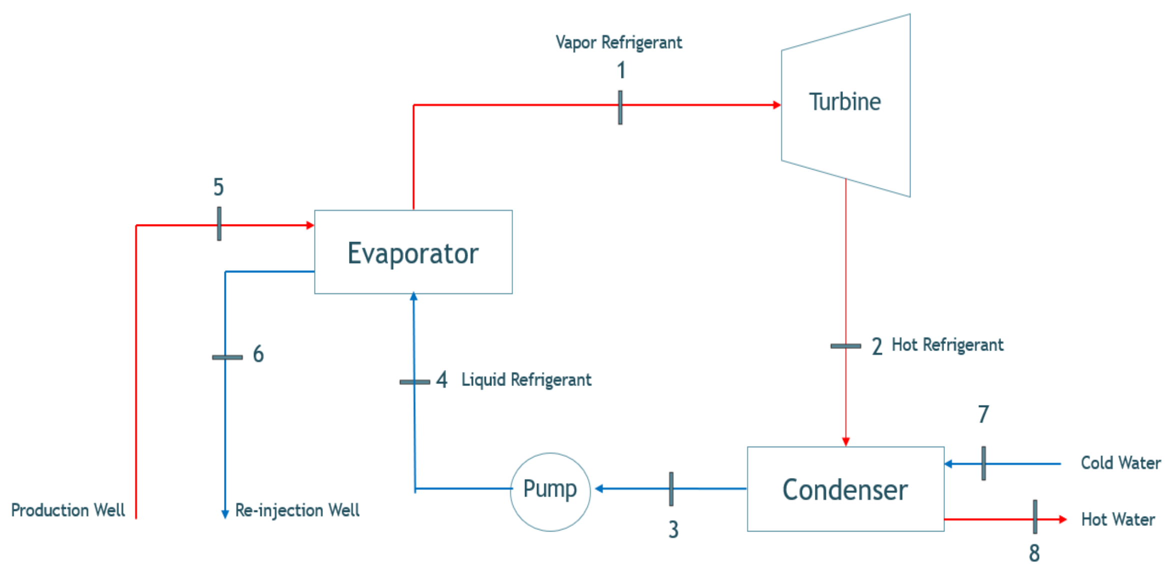

Figure 18. Organic Rankine Cycle schematic process.

The thermodynamic limit is set by Carnot Efficiency, but in real world the ORC net efficiencies are modest at low ΔT. Nonetheless ORCs effectively recover heat otherwise wasted, making them well-suited for medium-grade geothermal energy.

- $Carnot\ Efficiency = \eta_C = \frac{T_H - T_C}{T_H}$ **[Eq.3]**

Where T_H = Temperature of hot source and T_c = Temperature of Cold Source

3.1.1 Working Fluid for ORC

Selecting the working fluid is essential for ORC design. Two of the most frequently utilized fluids in contemporary ORCs are R-245fa (1,1,1,3,3-pentafluoropropane) and R-134a (1,1,1,2-Tetrafluoroethane) [81]. These HFC refrigerants possess boiling points and saturation characteristics appropriate for low to medium temperature sources. For instance, R-245fa features a critical temperature of approximately 154 °C and a pressure around 36.5 bar, with a normal boiling point of about 15.1 °C, enabling it to operate effectively in low- to medium-temperature heat sources. Similarly, R-134a has a critical temperature of 101.1 °C and a pressure around 40.6 bar, and a normal boiling point of approximately −26.1 °C, which makes it suitable for low-temperature geothermal applications [81]. It does not deplete the ozone layer (ODP=0), although it possesses a significant global-warming potential (GWP≈1050) [81]. In practice, R-245fa typically produces more net power than R-134a under identical conditions: one study indicated R-245fa provided approximately 4.7% greater power output than R-143a (R-123) in a low-temperature geothermal ORC [82]. Therefore, numerous plants have selected R-245fa (and R-134a) as standards.

3.1.2 Performance Modelling and Thermodynamic Equations

The ORC energy balance follows standard first-law relations. Denoting state points as shown in the figure 18, the steady-flow energy equations are all flows ought to be based on mass (m^*) and are the following [83]:

- $Heat\ Input\ (Evaporator) = Q_H = m^*\ (h3 - h2)$ **[Eq.4]**

- $Turbine\ Work = W_t = m^* (h3 - h4)$ **[Eq.5]**
- $Pump\ Work = W_p = m^* (h2 - h1)$ **[Eq.6]**
- $Net\ Power = W_{net} = W_t - W_p$ **[Eq.7]**
- $Thermal\ Efficiency = \eta_t = \frac{W_{net}}{Q_H}$ **[Eq.8]**

Where $m^* =$ mass and h = enthalpy

An exergy analysis can similarly be performed: one calculates exergy destruction in every component to pinpoint losses. In ORC facilities, exergy loss is mainly influenced by the heat exchangers (because of minor temperature differences) and the expander; contemporary designs focus on reducing pinch losses in the evaporator. Nonetheless, first-law efficiency continues to be the essential performance indicator for net power generation. Physical Exergy (E) is represented by the following Equation where h_0, s_0, and T_0 are the dead-state enthalpy, entropy and temperature respectively [83]:

- $E = m^*(h - h_0 - [T_0(s - s_0)$ **[Eq.9]**

The exergy destruction X_d balance Equations are the following [83]:

- $X_{d,Evap} = (E_4 + E_5) - (E_1 + E_6)$ **[Eq.10]**
- $X_{d,t} = (E_1) - (E_2 + W_t)$ **[Eq.11]**
- $X_{d,cond} = (E_2 + E_7) - (E_3 + E_8)$ **[Eq.12]**
- $X_{d,pump} = E_3 + W_p - E_4)$ **[Eq.13]**

Geothermal ORC plants have relatively low thermal efficiency due to modest temperature differences. A low-temperature ORCs (75–150 °C source) typically achieve electrical efficiencies of **5–12%** [84].

3.1.3 Environmental Analysis of ORC

Geothermal ORC energy has a significantly reduced environmental impact compared to fossil fuel production. Crucial elements consist of *(Figure 19)*:

<u>1.Greenhouse Gas and Air Emissions</u>: ORC binary plants do not combust fuel, resulting in virtually no on-site emissions of CO_2, SO_x, or NO_x. Only trace gases present

in the geothermal fluid (e.g. H_2S, CO_2) might be emitted, but these are usually insignificant. Life-cycle analyses indicate that, even with drilling and construction included, binary geothermal facilities release approximately 7–15 g CO_2/kWh [85]. For instance, the lifecycle analysis of the Rittershoffen (France) ORC plant indicates around 7–9 kg CO_2/MWh, while Iceland's Theistareykir plant shows approximately 14 kg CO2/MWh [85]. In contrast, a contemporary coal-powered facility releases approximately 800–1000 kg CO_2/MWh (while gas emits around 400–500 kg/MWh). Consequently, geothermal-ORC lowers carbon emissions by two orders of magnitude. It likewise produces no particulate matter or mercury contamination. One disadvantage is the environmental effect of the working fluid: R-245fa has a GWP of approximately 1050, necessitating tight sealing of systems or the use of lower-GWP alternatives [81].

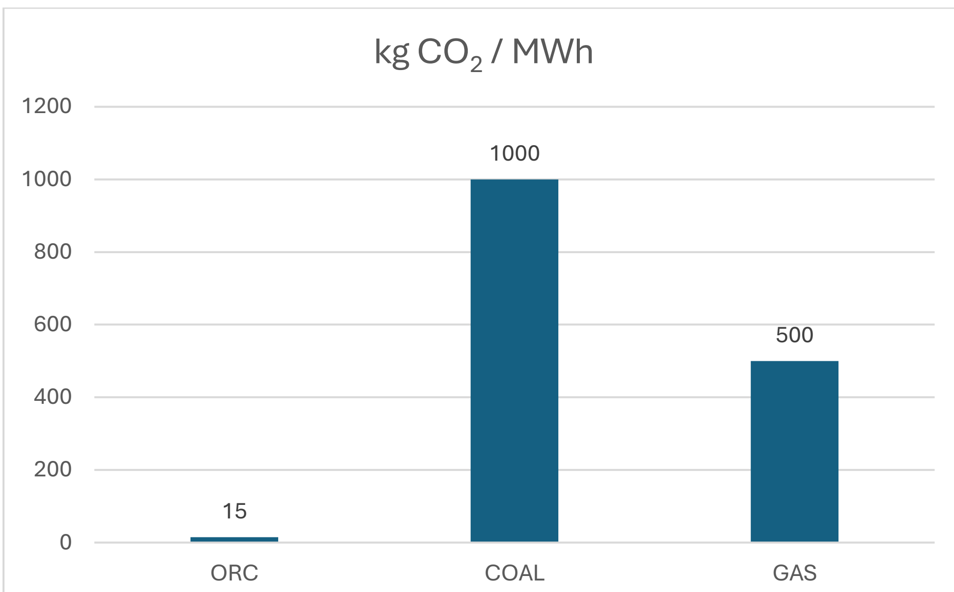

Figure 19. Difference in CO2 emissions of 3 power facilities

This shows that geothermal energy utilized for generating electricity through Organic Rankine Cycle will reduce the amount of CO2 by 98.5% and 97% with respect to that of coal and gas power plants respectively.

<u>2.Water Consumption</u>: ORC binary systems utilize minimal net water. The geothermal brine is sent back to the reservoir in a sealed cycle [86]. When air-cooling is utilized, almost no freshwater is used. When water cooling is implemented, it solely cools

the working fluid and not the geothermal brine, and it can even utilize wastewater. Fervo Energy states that their EGS ORC facilities utilize entirely non-potable water (brackish or recycled) and reinject all fluids completely [86]. In contrast, traditional steam plants extract significant amounts of water for cooling purposes. In 2015, U.S. thermoelectric facilities had an average water withdrawal of about 57 liters per kWh (mostly returned to the source) [87]. Geothermal binary ORCs therefore result in significantly reduced water stress.

Geothermal ORCs generate virtually no solid waste or ash. The noise and visual effects are moderate (like those of a small factory or substation). Risks are minimal: contemporary binary plants are enclosed and do not release heat or fluids to the surface. Regular monitoring addresses any brine gas (H_2S) or triggered seismic activity. In general, life-cycle assessments position geothermal (binary ORC) among the cleanest energy generation technologies regarding their total environmental impact [85].

3.2 Geothermal Driven Absorption Chiller

Geothermal absorption chillers utilize geothermal heat as the primary energy source to generate cooling via a thermally driven refrigeration method. In contrast to traditional vapor compression systems, absorption chillers need limited electrical energy, depending primarily on working fluid combinations like water–lithium bromide or ammonia–water. This technology is especially appropriate for geothermal resources with low to medium temperatures, facilitating effective cooling while minimizing electricity usage and greenhouse gas emissions. The major types are the following:

1. <u>Single-effect (one-stage)</u>: Generally powered by heat in the range of 85–110 °C. Employs a generator, absorber, condenser, evaporator, and solution pump. The typical working pair is $LiBr/H_2O$ (with water serving as the refrigerant). The usual COP (cooling coefficient-of-performance) is low, ranging from 0.5 to 0.7 [88]. Appropriate for moderate cooling capacity (tens to hundreds kW) when only medium-temperature geothermal resources are accessible.

2. Double-effect (two-stage): Features a high-pressure and low-pressure generator in series, enabling increased efficiency. Needs higher temperatures (100–200 °C). LiBr/H_2O is prevalent, often with additional substances [88]. COP increases to approximately 0.8–1.1 (frequently around 1.3–1.4 under design conditions) [88]. Requires approximately 150 °C to completely activate both phases. It is Utilized for cooling that requires greater capacity and improved efficiency.

3.2.1 Single Effect Absorption Chiller System Description

The primary components of the single-effect absorption refrigeration system include the generator, absorber, solution heat exchanger, evaporator, and condenser *(Figure 20)*. In this setup, the geothermal well acts as the primary heat source. Following the heat transfer via the heat exchanger, it flows into the system's generator. In the generator, a dilute solution is heated, producing high-temperature refrigerant vapor and a more concentrated solution. The high-temperature refrigerant vapor moves to the condenser, where it transforms into a high-pressure saturated liquid and expels heat to the cooling water. Following its passage through a throttling device to decrease pressure, the refrigerant liquid enters the low-pressure evaporator, where it takes in heat from the chilled water and transforms into a gaseous refrigerant. The gaseous refrigerant arrives at the absorber, where it is taken up by the concentrated solution and transformed into a dilute solution, emitting heat to the cooling water. The concentrated solution at high temperature from the generator and the dilute solution at low temperature from the absorber exchange heat in the solution heat exchanger. The generator receives the dilute solution, while the concentrated solution goes into the absorber, finishing the cycle.

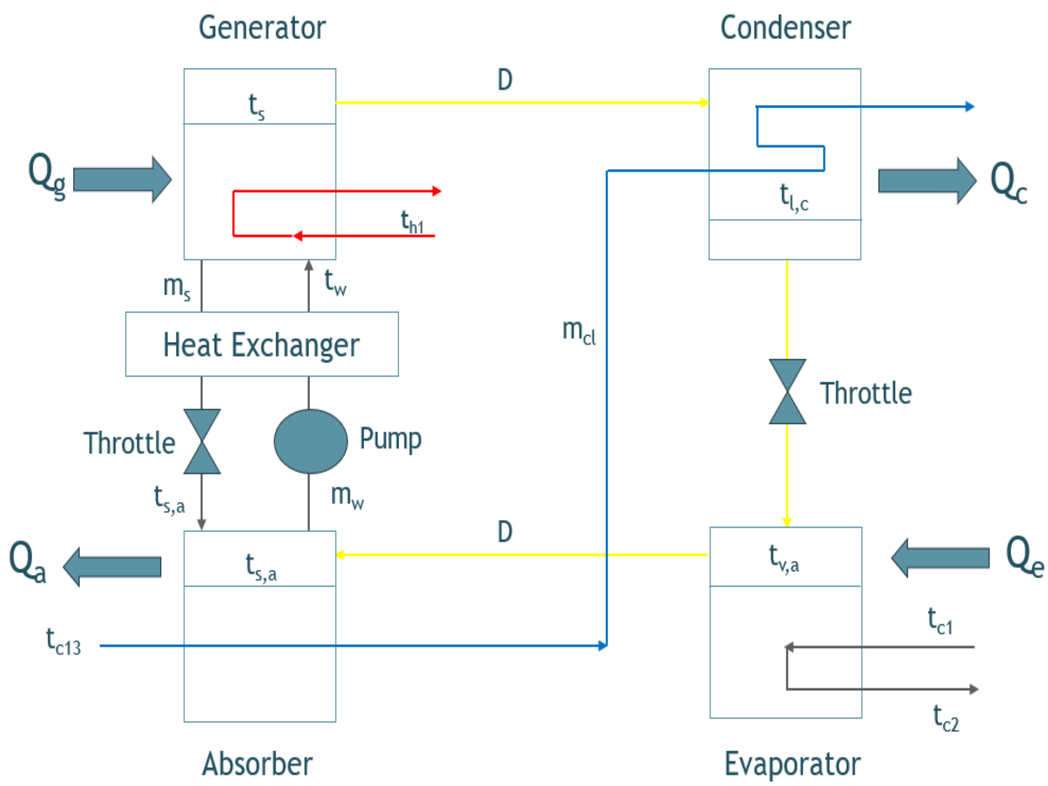

Figure 20. The process of single absorption chiller

3.2.2 Modelling of the Single-Effect Absorption Chiller

Generator Modelling: Inside the generator, the dilute solution takes in the heat emitted by the driving heat source, leading some of the water in the solution to vaporize into gas and leave the generator [88]. The diluted solution gets concentrated and returns to the solution heat exchanger, with the mass of the solution entering and going out being equal at any specific instant [88], conforming to the principle of mass conservation, described as follows [88]:

➢ $m_w = m_s + D$ **[Eq.14]**

The energy entering the generator consists of the energy from the dilute solution and the heat emitted by the driving heat source. The total of the two mentioned equals the combined energy of the vaporized working fluid and the concentrated solution. Simultaneously, the energy taken in or given off by the working fluid as it enters and exits the generator adheres to the principle of energy conservation along with the heat source, represented as follows [88]:

➢ $m_w h_{w,g} + Q_g = D h_{v,g} + m_s h_s$ **[Eq.15]**

In addition to that, $t_s = t_{h1} - \Delta t_s$ exits the generator, where Δt_s is the heat transfer temperature difference of the generator [88].

Condenser Modelling: The working fluid which enters the condenser heats with the cooling water, and its energy conservation is as follows [88]:

➢ $Q_c = D(h_{v,g} - h_{l,c})$**[Eq.16]**

In addition to that, $t_{l,c} = t_{cl3} + \Delta t_{l,c}$ exits the condenser, where $\Delta t_{l,c}$ is the heat transfer temperature difference of the condenser [88].

Evaporator Modelling: Like the condenser, in the evaporator, the quality of the circulating working fluid entering and exiting the evaporator remains consistent, as the working fluid transfers heat to the chilled water, represented as follows [88]:

➢ $Q_e = D(h_{v,a} - h_{l,c})$ **[Eq.17]**

In addition to that, $t_{v,a} = t_{c2} + \Delta t_{v,a}$ exits the condenser, where $\Delta t_{v,a}$ is the heat transfer temperature difference of the Evaporator [88].

Absorber Modelling: In the absorber, the circulating working fluid combines with the concentrated solution that has left the generator and experienced heat exchange in the solution heat exchanger, transforming into a dilute solution prior to reentering the solution heat exchanger. The energy variation between the inflow and outflow of the working fluid is the heat transfer Q_a with the cooling water, defined as follows [88]:

➢ $Q_a = m_w h_w - m_s h_{s,a} - D h_{v,a}$ **[Eq.18]**

Heat Exchanger Modelling: In the solution heat exchanger, heat is exchanged between the concentrated solution and the dilute solution. The heat exchange rate of the solution is assumed to be constant, based on this the mass that enters and left the solution heat exchanger must be balanced, as determined below [88]:

➢ $m_w X_w = m_s X_s$ **[Eq.19]**

➢ $m_s(h_s - h_{s,a}) = m_w(h_{w,g} - h_w)$ **[Eq.20]**

In addition to that, the solution heat exchanger has the same temperature difference heat formula $t_{s,a} = t_w + \Delta t_{s,a}$, where $\Delta t_{s,a}$ is the heat transfer temperature difference of the Heat Exchanger [88].

3.2.3 System Evaluation

Throughout the entire system, the quality of the working fluid circulating in and out of both the condenser and evaporator remains consistent. The flow of the working fluid is consistently D as in figure 20. Furthermore, in the system, the heat taken in by the cooling water equals the heat emitted by the driving heat source and the chilled water [88].

➢ $Q_g + Q_e = Q_a + Q_c$ **[Eq.21]**

The COP of the refrigeration system is the proportion of the heat taken in by the evaporator to the heat emitted by the driving heat source and the energy used by the solution pump (W_p) [88].

➢ $COP = \frac{Q_e}{Q_g + W_p}$ **[Eq.22]**

The efficiency of the refrigeration system is quantified by COP, while the effectiveness is evaluated using ECOP. The ECOP system is the ratio of the exergy produced by the evaporator to the total exergy of the input generator system and the energy used by the solution pump, expressed in terms of temperature [88].

➢ $$ECOP = \frac{Q_e\left(\frac{1-\left(t_{l,c}+273.15\right)}{\left(t_{v,a}+273.15\right)}\right)}{Q_g\left(\frac{1-\left(t_{l,c}+273.15\right)}{\left(t_s+273.15\right)+W_p}\right)}$$ **[Eq.23]**

From the analysis provided, it can be inferred that in a single-effect absorption refrigeration system, there exist thermodynamic and heat transfer interactions among the five primary heat transfer elements. The system's COP and ECOP rise with an increase in refrigeration water inlet temperature, a higher cooling water flow rate, a greater charging concentration, and a decrease in cooling water inlet temperature, respectively. Nonetheless, ECOP reduces as the temperature of the heat source rises [88].

3.2.4 Environmental Impact: Emissions and Energy Use

Geothermal energy is nearly free from carbon emissions: Extracting fluid from the earth at 90–150 °C produces almost no CO_2 or other greenhouse gases. The primary energy expense is the pump power, which can be provided by renewable sources or low-carbon grid electricity [87]. While in electric chillers the amount of GHG emitted is related to the amount of electricity consumed which has direct relation with the carbon intensity factor of the grid, in addition to the COP of the electric chiller, since COP is the ratio of cooling output (in kW) to electrical energy input (in kW).

Primary energy savings: Since geothermal heat avoids losses from power plants, its direct application results in significant primary-energy conservation. In practice, systems employing absorption chillers powered by geothermal-waste heat demonstrate substantial savings in primary energy and CO_2 emissions. For example, studies of hybrid geothermal-cooling facilities have discovered approximately 95% decrease in primary energy consumption and about 95–97% decline in CO_2 emissions when compared to traditional grid-cooled systems [89]. Additionally, LiBr/H_2O systems utilize water as a refrigerant, which has no potential for Ozone Depletion Potential or Global Warming Potentital, in contrast to numerous compression cycles. In practice, absorption chillers fueled by low-cost thermal sources typically consume less overall primary energy than electric chillers powered by the grid. Analysis indicates that despite a reduced numerical COP, the operational cost and net fuel consumption of an absorption system can be lower when inexpensive thermal energy is accessible [90].

As a conclusion, energy performance (COP) of absorption chillers is lower than that of electric chillers, but the primary energy efficiency and GHG impact are often better for geothermal/absorption systems due to the use of renewable heat source. Thus, for industrial cooling using available medium-enthalpy geothermal heat, absorption chillers offer a sustainable option compared to electric compressors, with thorough analysis demonstrating considerable benefits in CO_2 emissions and primary energy usage.

3.3 Geothermal Heating Process

District heating is a modern energy conveyance and distribution network utilized for warmth indoor environments *(Figure 21)*. Energy is produced by utilizing a renewable source, frequently located several km away from its point of use. Essential elements of district heating consist of co-generation facilities, where heat is generated and then distributed through a network that connects individual residences [91]. These systems are uniquely designed to function remotely and have the intrinsic ability to harness a subsurface resource, specifically geothermal energy.

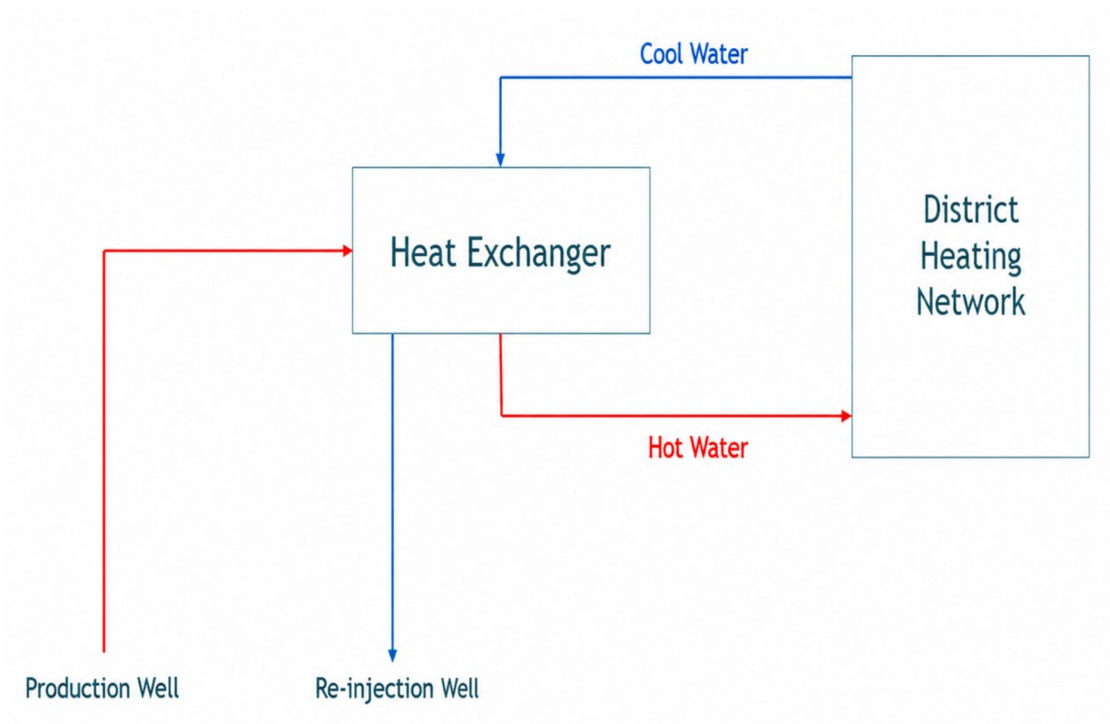

Figure 21. The process of tapping geothermal energy for heating

3.3.1 Thermal Energy Performance Analysis

A geothermal district heating system extracts thermal energy from deep underground reservoirs and passes it through heat exchangers then distributed to a piping network through substations to feed buildings, industries, or commercial complexes. The thermal power extracted (Q) is given by the flow rate multiplied by specific heat and temperature drop.

➢ $Q = m^{*} C_p \Delta T$ **[Eq.24]**

m^{*}= flow rate (kg/sec)

C_p = Specific heat capacity (J/kg×K)

ΔT = Temperature drop between the supply and return heat source (K).

Optimizing the thermal energy extracted depends on the design of heat exchanger, which is in direct relation with the temperature of heat source [92] *(Figure 22)*. Thus, optimizing the design leads to the highest effectiveness of heat exchanger which yields the highest thermal efficiency obtained [92].

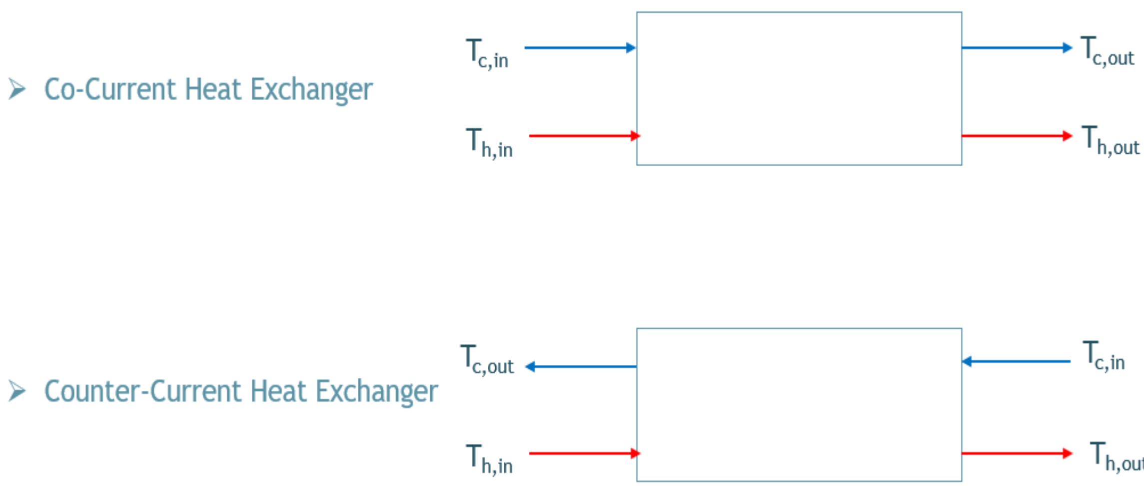

Figure 22. Different types of heat exchangers

<u>1. Counter-Current flow Heat exchanger:</u> Counter-current flow heat exchangers exchange heat between two fluids moving in opposite directions, with one fluid being the hot geothermal fluid (T_h) and the other a purified circulating fluid (T_c). The output temperature of the geothermal fluid was determined based on the input temperatures entering the heat exchanger [92]:

$$➢\ T_{h,out} = T_{h,in} - \left(T_{h,in} - T_{c,in}\right) - \frac{(1-e^D)}{\left(\left(\frac{C_h}{C_c}\right)-e^D\right)}$$ **[Eq.25]**

Where T is the temperature, C is the thermal capacity, and D is calculated as $D = U \times A\ (\frac{1}{C_h} - \frac{1}{C_c})$, where U is the heat transfer coefficient and A is the heat transfer area [92]. The thermal capacity was as $C = m^* \times C_p$ [92].

The temperature of the cold fluid circulating after heat transfer is calculated assuming that the heat transfer rate of the geothermal fluid is known, as follow [92]:

$$➢\ C_h\left(T_{h,in} - T_{h,out}\right) = C_c(T_{c,in} - T_{c,out})$$ **[Eq.26]**

The effectiveness (ε) is expressed as values between 0 and 1, where 0 represents ineffective and 1 represent 100% effective, and it is calculated as follow [92]:

$$➢\ \varepsilon = \frac{(1-e^D)}{\left(\left(\frac{C_h}{C_c}\right)-e^D\right)}$$ **[Eq.27]**

<u>2.Co-Current Flow Heat Exchanger</u>: Involves the transfer of heat between 2 fluids travelling in the same direction. The outlet temperature of the heat source is calculated as follows [92]:

$$➢\ T_{h,out} = T_{c,in} + \frac{(T_{h,in}-T_{c,in})}{\left(1+\left(\frac{C_c}{C_h}\right)\right)\left(1-e^{-\frac{U.A}{C_c}}\right)}$$ **[Eq.28]**

Where also the effectiveness (ε) is calculated as follow [92]:

$$➢\ \varepsilon = \left(\frac{C_h}{C_c}\right).\left(1 - \frac{1}{\left(1+\left(\frac{C_c}{C_h}\right)\right)\left(1-e^{-\frac{U.A}{C_c}}\right)}\right.$$ **[Eq.29]**

Generally, counter-current flow heat exchangers are utilized in heat networks because of their superior efficiency; nonetheless, co-current flow heat exchangers were also analyzed for comparison [92].

3.3.2 Environmental Impact Analysis

Geothermal heating exhibits a significantly low life-cycle carbon intensity. An IPCC review indicates that the life-cycle emissions for geothermal district heating range from approximately 14 kg CO_2-eq/MWh_{th} [93]. In contrast, traditional fossil fuel heat sources release around ten times more CO_2, with natural gas furnaces emitting about 185 kg CO_2/MWh and oil boilers releasing roughly 245 kg CO_2/MWh [94] (*Figure 23)*.

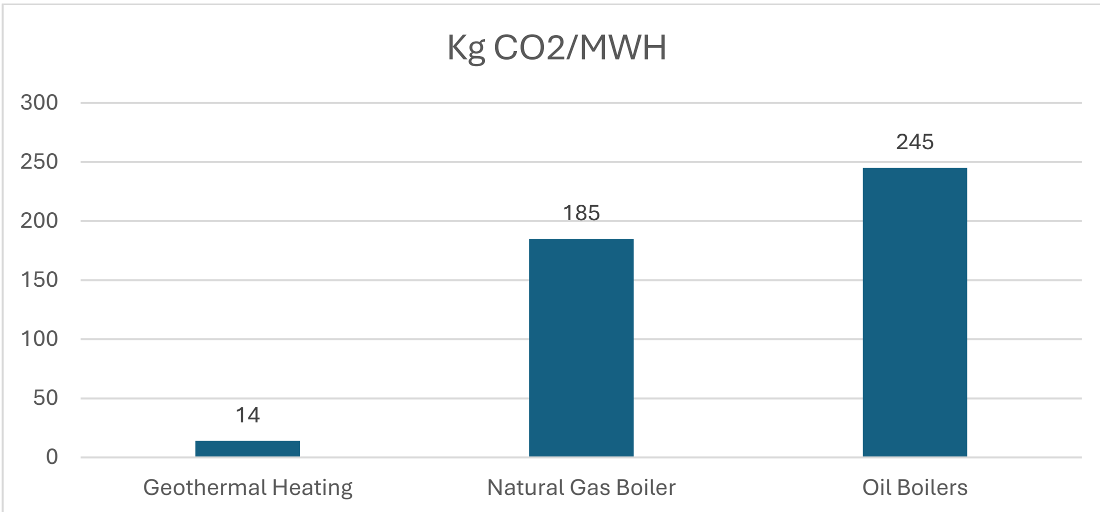

Figure 23. Amount of CO2 emitted by different technologies

This implies that Geothermal Heating system reduces the amount of CO2 emitted by 92.4% compared to natural gas boilers, and by 94.2 % compared to oil boilers. Surface emissions of other gases from a well are generally minimal for non-volcanic reservoirs. If the geothermal fluid has dissolved gases (H_2S, CH_4, etc.), contemporary systems isolate and reinject them; direct emissions are minimized or managed through mitigation. The IPCC observes that geothermal brine is typically reinjected to maintain reservoir pressure and avoid contamination [93].

This proves that integration of geothermal energy with heating process is clean process that helps in strongly reducing the environmental impacts with respect to traditional heating process.

Chapter 4: Case Study of Data Center Cooling System Design in Emilia-Romagna Region Utilizing the Geothermal Potential in Ferrara

In this chapter it will be conducted a case study involving the design of a data center that will utilize geothermal energy for cooling. Simulation, modeling, and optimization of the process will be carried out by using Aspen Hysys. Data Center cooling requires around 40% of its annual energy consumption, which can be also related to the use of huge amounts of water to supply this requirement [95]. Thus, in this chapter it will be figured out the processes that can be integrated with the Ferrara medium enthalpy geothermal system. This includes extracting and analyzing the needed parameters of the geothermal system, implementing either ORC or Geothermal Absorption Chiller for the cooling process of data center.

4.1 Ferrara Geothermal Reservoirs

The reservoir formation consists of Mesozoic brecciated medium-grained dolomite. The upper geothermal reservoir (25%) is situated between 1,170 m and 1,390 m, while the lower one (67%) occurs from 1,790 to 1,960 m [96]. The fluid has a temperature almost steady at 100° C from 1,250 to 1,960 m, with a salinity of 65 g/l. The total flowrate of the geothermal plant is 400m^3/hr (~111 kg/sec), while the thermal nominal power is 14 MW$_{th}$ and thermal energy produced is 75 GWh/year (75,000 MWh/year) [97]. *Table 5* summarizes the data above.

Table 5. Parameters and Values of Ferrara Geothermal reservoirs.

Parameter	Value
Reservoir Lithology	Mesozoic brecciated medium-grained dolomite
Upper Reservoir Depth	1,170–1,390 m

Upper Reservoir Contribution	25%
Lower Reservoir Depth	1,790–1,960 m
Lower Reservoir Contribution	67%
Reservoir Temperature	~100 °C (from 1,250 to 1,960 m)
Fluid Salinity	65 g/L
Fluid Composition at Surface	H_2S: 0.2 g/L; CO_2: 0.47 g/L; traces of hydrocarbons (N_2 + CH_4)
Total Flowrate	400 m³/h (~111 kg/s)
Thermal Nominal Power	14 MW_{th}
Annual Thermal Energy Production	75 GWh/year (75,000 MWh/year)

4.2 Process simulation

As the motivation of current study involves investigating the optimal utilization of a geothermal energy source for data center cooling applications, the available geothermal resource consists of a water outlet stream with a flow rate of 400 m^3/hr, carrying 14 MW of thermal energy, with a specific salinity content. Two distinct thermodynamic cycles will be evaluated to determine the most efficient conversion pathway: a direct cooling approach using a Lithium Bromide (LiBr) absorption chiller, and an indirect approach employing an Organic Rankine Cycle (ORC) to produce electricity which can be utilized to run the electric chiller. Both systems will be rigorously modeled using industry-standard process simulation software to ensure accurate performance predictions under the specified geothermal source conditions.

The LiBr absorption chiller system will be simulated in Aspen Plus, utilizing the geothermal hot water as the heat source to drive the absorption refrigeration cycle, which directly produces chilled water for data center cooling. In parallel, the Organic Rankine

Cycle will be modeled in Aspen HYSYS, where the geothermal energy first generates electrical power through the ORC turbine-generator system, which is then used to operate conventional electric chillers. Following comprehensive simulation of both configurations, a detailed comparative analysis will be conducted based on key performance metrics including cooling capacity output, overall energy efficiency, coefficient of performance (COP), and practical considerations such as system complexity and maintenance requirements. The energy outputs from both approaches will be quantitatively compared to identify the best technology for this specific geothermal resource and data center cooling application, ultimately providing a data-driven recommendation for system implementation.

4.3 Organic Rankine Cycle Simulation

The Organic Rankine Cycle (ORC) system has been simulated in Aspen HYSYS using iso-pentane as the working fluid and the Peng-Robinson thermodynamic property package which is most suitable for hydrocarbon-based refrigerant systems operating under specified conditions. The geothermal hot water stream enters the system at 100°C with a flowrate of 400 m^3/hr and serves as the primary heat source for the dual-loop ORC configuration. In section 3.1, the simple Organic Rankine Cycle was discussed but to maximize the use of the heat from geothermal energy a dual loop arrangement was taken into consideration. This dual-loop arrangement is specifically designed to maximize heat recovery from the geothermal water stream and maximize electricity generation by utilizing two parallel iso-pentane cycles operating at different pressure levels, allowing for more efficient extraction of thermal energy across the temperature gradient of the cooling water stream *(Figure 24)*.

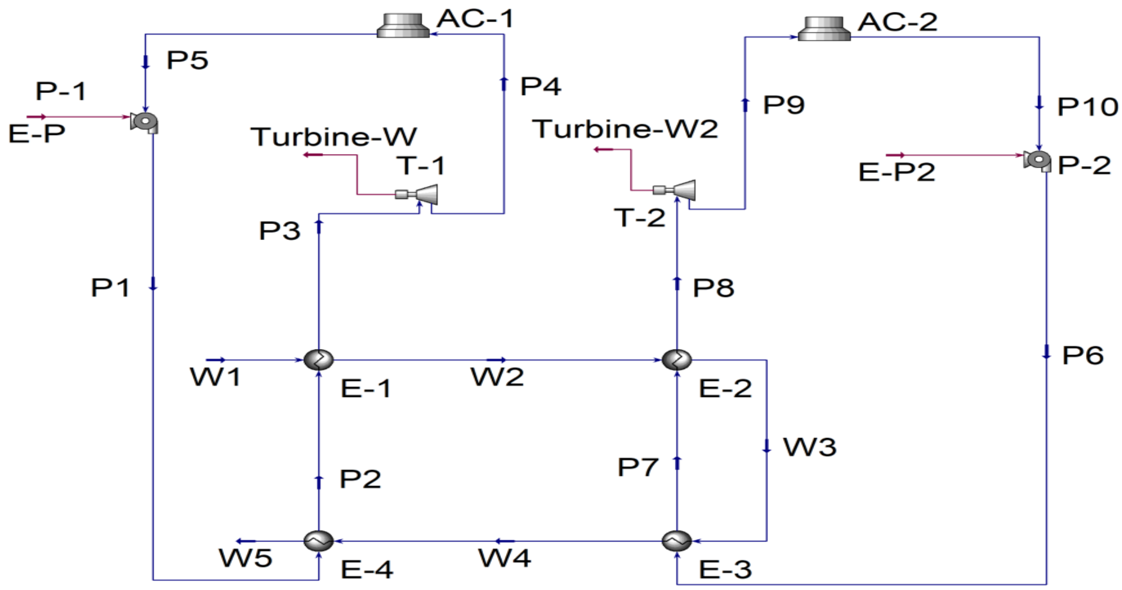

Figure 24. Simulation of the dual loop ORC process

Geothermal water (W1) enters the first heat exchanger E-1, where it transfers heat to the first iso-pentane loop, and subsequently flows through E-2, E-3, and E-4 in series, progressively transferring its thermal energy to both iso-pentane loops. In the first loop, iso-pentane stream P1 is heated and vaporized in heat exchangers E-4 and E-1, with the superheated vapor (P3) expanding through turbine T-1 to generate electrical power while the turbine exhaust stream (P4) is directed for further processing. The second iso-pentane loop follows a similar thermodynamic path, where stream P6 is heated and vaporized in heat exchangers E-2 and E-3, with the resulting high-pressure vapor (P8) expanding through turbine T-2 to produce additional electricity, and the turbine exhaust stream (P9) exits for subsequent cooling. This cascaded heat exchange configuration ensures that the geothermal water is cooled progressively from W1 through W2, W3, W4, and finally to W5, achieving maximum thermal energy extraction from the available heat source.

Following power generation in the turbines, the expanded iso-pentane vapor streams are cooled using air coolers AC-1 and AC-2, which reject waste heat to the atmosphere and convert the vapor streams P4 and P9 into saturated liquid streams P5 and P10, respectively. These condensed iso-pentane streams are then pressurized by pumps P-

1 and P-2, which raise the pressure of streams E-P and E-P2 to the required levels for re-entry into the heat exchangers network, thus completing the closed thermodynamic cycles. The two independent iso-pentane loops operate continuously, with each loop comprising heating, expansion, cooling, and pumping stages that work in parallel to extract maximum available work from the geothermal heat source. The detailed streams data of the ORC process is represented below in Table 6,7, and 8.

Table 6. Data of the geothermal water streams of ORC

Parameter/Stream	W1	W2	W3	W4	W5
Vapor Fraction	0.0	0.0	0.0	0.0	0.0
Temperature (°C)	100.0	79.7	77.2	76.4	72.3
Pressure (bar)	30.0	29.5	29.0	28.5	28.0
Molar Flow (kmol/h)	22158.9	22158.9	22158.9	22158.9	22158.9
Mass Flow (kg/h)	399194.4	399194.4	399194.4	399194.4	399194.4
Volume Flow (m^3/h)	400.0	400.0	400.0	400.0	400.0

Table 7. Data of 1st isopentane streams of ORC

Parameter/Stream	P1	P2	P3	P4	P5
Vapor Fraction	0.0	0.0	1.0	1.0	0.0
Temperature (°C)	27.9	60.0	98.3	61.4	27.5
Pressure (bar)	7.5	7.4	6.9	1.0	1.0
Molar Flow (kmol/h)	1300.0	1300.0	1300.0	1300.0	1300.0
Mass Flow (kg/h)	93796.3	93796.3	93796.3	93796.3	93796.3
Volume Flow (m^3/h)	150.4	150.4	150.4	150.4	150.4

Table 8. Data of 2nd isopentane streams of ORC

Parameter/Stream	P6	P7	P8	P9	P10
Vapor Fraction	0.0	0.0	1.0	1.0	0.0

Temperature (°C)	27.7	67.0	62.5	43.5	27.5
Pressure (bar)	4.0	3.9	2.9	1.0	1.0
Molar Flow (kmol/h)	200.0	200.0	200.0	200.0	200.0
Mass Flow (kg/h)	14430.2	14430.2	14430.2	14430.2	14430.2
Volume Flow (m^3/h)	23.1	23.1	23.1	23.1	23.1

The flowrate of water stream from the geothermal source is fixed at 400 m^3/hr with temperature of 100 °C, and the flowrate of iso-pentane is setto 1300 kmol/hr to maximize electricity output of the process. The heat exchanger's equipment data is presented below in Table 9 for all four exchangers selected as shell and tube heat exchanger, while placing iso-pentane on tube side and hot water at shell side.

Table 9. Data related to the heat exchangers flow

Heat Exchanger	*Unit*	**E-1**	**E-2**	**E-3**	**E-4**
Duty	*kJ/h*	35467441.90	4379832.67	1343157.43	7042967.43
Tube Side Feed Mass Flow	*kg/h*	93796.30	14430.20	399194.41	399194.41
Shell Side Feed Mass Flow	*kg/h*	399194.41	399194.41	14430.20	93796.30
Tube Inlet Temperature	*°C*	60.00	67.00	77.16	76.40
Tube Outlet Temperature	*°C*	98.30	62.50	76.40	72.35
Shell Inlet Temperature	*°C*	100.00	79.68	27.65	27.87
Shell Outlet Temperature	*°C*	79.68	77.16	67.00	60.00

The pumps are used to increase the pressure of the iso-pentane circulating in the loops, for major iso-pentane loop pressure is increased to 7.5 bar and for secondary loop pressure is 4 bar. The detailed power consumption along with capacity data for pumps is presented below in Table 10.

Table 10. Data consumption of Pumps

Pumps	*Unit*	**P-1**	**P-2**

Power	*kW*	36.80	2.61
Capacity (Actual Vol. Flow)	*m^3/h*	152.85	23.51
Feed Pressure	*bar*	1.00	1.00
Product Pressure	*bar*	7.50	4.00
Product Temperature	*°C*	27.87	27.65

After exchanging the heat with the hot water in the exchangers the iso-pentane is vaporized and sent to the turbines. The turbines are the main simulated equipment which leads us towards power generation. The vaporized iso-pentane circulating in the loops produces electricity when it moves turbine. The detailed power generation data along with capacity data for both turbines is presented below in Table 11.

Table 11. The power generation data of turbines

Turbines	*Unit*	**Turbine-1(T-1)**	**Turbine-2(T-2)**
Power Produced	*kW*	1386.33	112.34
Capacity (Vol flow)	*m^3/h*	4847.98	1756.19
Feed Pressure	*Bar*	6.90	2.90
Product Pressure	*Bar*	1.00	1.00
Product Temperature	*°C*	61.37	43.47

- $Power\ generated\ = 1386.33 + 112.34 = 1498.67\ kW = 1.49867\ MW$

As this power is going to be utilized by the electric chillers for cooling of data center. For industrial/data center electric chillers, a COP value of 4.0 to 6.5 is typical for water-cooled systems [98], with 4.5 being a reasonable limit assumption for chillers. So, the actual cooling produced by the power generated by ORC is calculated as follows.

- $Cooling\ duty\ produced = 1.49867\ MW * COP$ **[Eq.30]**

$$Cooling\ duty\ produced = 1.49867\ MW * 4.5 = 6.744015\ MW$$

4.4 Absorption Chiller Simulation

The Lithium Bromide (LiBr) absorption chiller system has been simulated in Aspen Plus using the Electrolyte NRTL-RK property package, which is the most suitable for this system as LiBr dissociates into ions during the absorption process and requires accurate modeling of electrolyte thermodynamics. The process is presented in *Figure 25*. The dilute solution containing LiBr and water enters the pump at 32.7°C as stream 1, where it is pressurized and exits as stream 2. This pressurized dilute solution then passes sequentially through a series of heat exchangers—COLD, HX-1, and HX-2—where its temperature is progressively raised from 32.7°C to 78.34°C through internal heat integration with the hot strong solution returning from the generator.

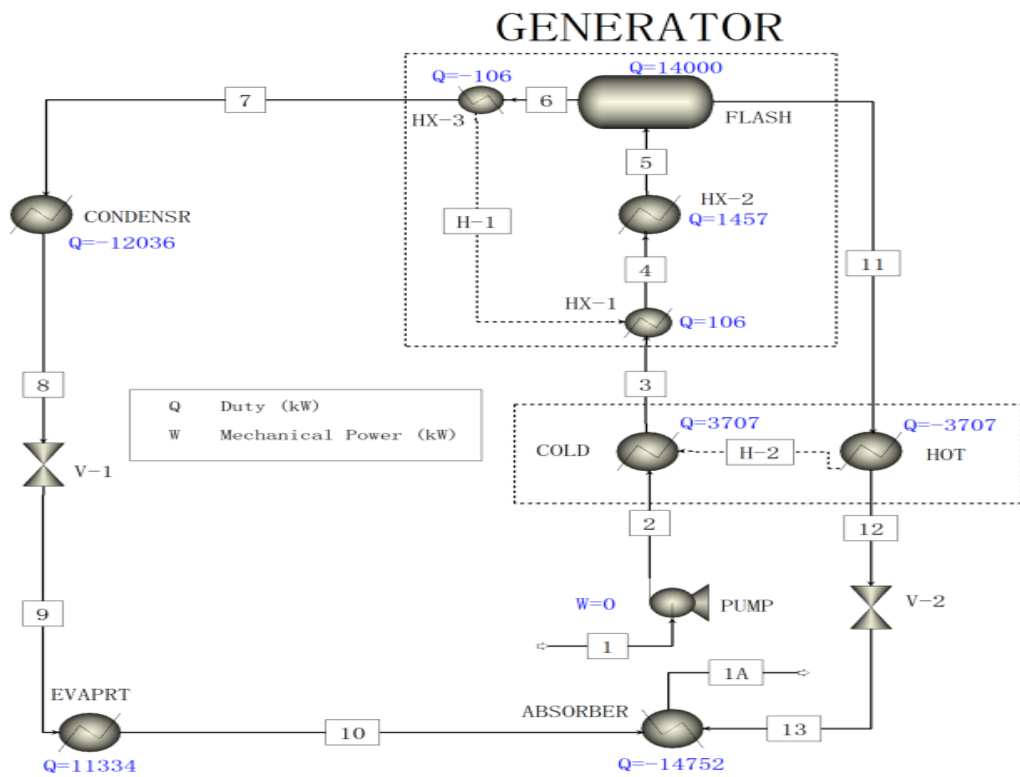

Figure 25. Simulation process of LiBr Absorption Chiller

The preheated dilute solution enters the generator (FLASH) as stream 5 at 78.34°C, where the 14 MW thermal energy from the geothermal source is applied (Q=14000 kW) to drive the separation process. Inside the generator, the heat input causes the water to evaporate from the lithium bromide solution, resulting in two distinct outlet streams: stream 6 containing pure water vapor at elevated temperature and stream 11 containing the highly concentrated solution of LiBr and residual water. The solution stream 11, now having a higher concentration of lithium bromide, is recycled back into the system after appropriate cooling and heat integration, where it exchanges heat with the incoming dilute solution through the HOT heat exchanger (Q=-3707 kW) and COLD heat exchanger (Q=3707 kW) to improve overall system thermal efficiency.

The water vapor stream 6 exiting the generator flows to the condenser, where it is cooled and condensed into liquid water at 40°C. The condensed water stream 8 then passes through valve V-1, which significantly reduces the pressure of the stream to create the low-pressure conditions required for the evaporation stage, producing stream 9. This pressure reduction is essential for enabling the refrigerant water to evaporate at low temperatures in the subsequent evaporator unit, thereby generating the desired cooling effect for the data center application.

The low-pressure liquid water stream 9 enters the evaporator, where it absorbs heat from the cooling load and evaporates, producing the useful cooling duty of Q=11,334 kW that will be utilized for data center cooling. The evaporated water stream 10 then flows to the absorber, where it is absorbed by the concentrated LiBr solution stream 12 that enters the absorber after passing through valve V-2 from the generator loop. The absorption process is highly exothermic and releases heat (Q=-14,752 kW) that must be rejected to maintain the absorber at low temperature and sustain the absorption process. ‘The resulting stream 13 enter the absorber, meet stream 12, and is fed back to the pump as stream 1 (stream 1A is identical to stream 1), completing the closed thermodynamic cycle. The pump's mechanical work is indicated as zero in the Aspen Plus results since it is negligible in relation to the thermal energy transfers in the system. In absorption cycles, the working fluid remains in the liquid state, characterized by a very low specific volume; consequently, the energy needed for pumping to raise its pressure is minimal. Consequently, this effect is frequently approximated as zero or disregarded in simulations, because it is minimal compared to the system's heating and cooling requirements.

Simulation, streams, and heat transfer results and outputs are summarized in Tables 12, 13, 14 and 15.

Table 12. Stream results of absorption chiller

Streams	Units	**1**	**1A**	**2**	**3**	**4**	**5**	**6**
From			ABSORBER	PUMP	COLD	HX-1	HX-2	FLASH
To		PUMP		COLD	HX-1	HX-2	FLASH	HX-3
Temperature	°C	32.70	32.70	32.70	64.81	65.72	78.34	89.90
Pressure	bar	0.01	0.01	0.07	0.07	0.07	0.07	0.07
Vapor Fraction		0.00	0.00	0.00	0.00	0.00	0.00	1.00
Mole Flows	kmol/hr	7801.16	7801.16	7801.16	7801.16	7801.16	7801.16	970.18
Volume Flow	m^3/hr	133.19	133.19	133.19	135.12	135.19	136.22	392286.55

Table 13. Stream result of absorption chiller

Streams	Units	**7**	**8**	**9**	**10**	**11**	**12**	**13**
From		HX-3	COND	V-1	EVAPRT	FLASH	HOT	V-2
To		COND	V-1	EVAPRT	ABSOR	HOT	V-2	ABSOR
Temperature	°C	78.40	40.20	1.23	1.31	89.90	53.30	43.15
Pressure	bar	0.07	0.07	0.01	0.01	0.07	0.07	0.01
Vapor Fraction		1.00	0.00	0.07	1.00	0.00	0.00	0.01
Mole Flows	kmol/hr	970.18	970.18	970.18	970.18	6830.98	6830.98	6830.98
Volume Flow	m^3/hr	379841.52	17.62	215494.63	3292854.2	119.70	117.11	299221.91

Table 14. Heat exchanger data for absorption chiller

Heat Exchanger	*Unit*	**COLD**	**HOT**	**HX-1**	**HX-2**	**HX-3**
Duty	*kW*	3707	-3707	106.47	1457	-106.47
Mass Flow	*kg/h*	211611	194133	211611	211611	17478
Outlet Temperature	*°C*	64.80	53.30	65.72	72.35	78.4
Outlet Pressure	*bar*	0.07461	0.07461	0.07461	0.07461	0.07461

Table 15. Results of the generator

Outlet temperature	*°C*	89.9
Outlet pressure	Bar	0.07461
Vapor fraction		0.124363
Net duty	kW	14000

Power generated by the evaporator as cooling duty is denoted as the following:

- $Q = 11334\ kW = 11.334\ MW$

4.4.1 Thermodynamic discussion of Utility Deviations

The notable gap between real and expected utility usage suggests that the LiBr–H_2O absorption chiller functions significantly beneath its thermodynamic ideal. In this research, the real utility usage denotes the heating and cooling loads directly derived from the Aspen Plus simulation outcomes based on the established base-case operating conditions, which encompass defined temperatures, pressures, and equipment performance metrics. These relate to 26,790 kW for both heating and cooling services, as indicated in *Figure 26*. Conversely, the desired (target) utility usage signifies the lowest theoretical utility requirement, calculated via process integration analysis using the same Aspen Plus model, presuming enhanced heat recovery and minimizing thermodynamic irreversibility. These target values (15,110 kW for heating and 15,100 kW for cooling) represent the optimized energy needs achieved by reducing external utilities. Absorption systems mainly rely on thermal energy instead of electricity, so their effectiveness is significantly affected by internal heat recovery, temperature operating levels, and cycle inefficiencies, which clarifies the difference between simulated (actual) and optimized (target) utility usage.

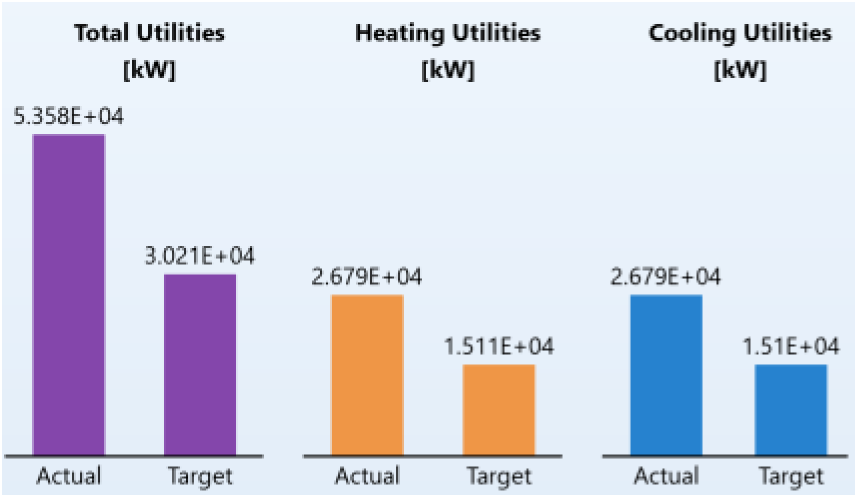

Figure 26. Difference between actual and target utilities

A key performance indicator is the **coefficient of performance (COP)**, defined as:

$$➢ \; COP = \frac{Q_{evap}}{Q_{gen}} \text{ [Eq.31]}$$

where Q_{evap} is the cooling effect and Q_{gen} is the heat supplied to the generator. The high actual heating utility demand, which is 26,790 kW, suggests that more thermal energy is being supplied to the generator than the one that would be required under optimal conditions. This typically indicates:

- Low solution heat exchanger effectiveness, causing inadequate preheating of the highly concentrated solution before entering the generator
- Higher-than-necessary generator temperature, which increases heat input without a proportional gain in cooling capacity
- Internal irreversibility due to poor heat and mass transfer in the generator

At the same time, the cooling utility demand (26,790 kW actual vs. 15,100 kW target) reflects excessive heat rejection in the **condenser and absorber**. Thermodynamically, this points to:

- Elevated absorber and condenser temperatures, often caused by high cooling water temperatures or insufficient heat transfer area
- Reduced absorption efficiency, which forces more heat to be rejected per unit of cooling produced
- Higher circulation ratio of the LiBr solution, increasing the thermal load that must ultimately be rejected

In an absorption cycle, since almost all the heat provided to the generator needs to be released in the absorber and condenser, comparable amounts of heating and cooling utilities are anticipated. Nonetheless, the reality that both are approximately 77% above the target indicates that the problem is widespread rather than limited to one specific part. While from a second law (exergy) perspective, the system is likely experiencing significant exergy destruction due to:

- Large temperature differences in heat exchangers
- Mixing and mass transfer irreversibility in the absorber
- Non-ideal heat recovery between strong and weak solution streams

4.4.2 Environmental Analysis of Absorption Chiller

The Lithium Bromide-Water (LiBr-H_2O) absorption chiller system offers significant environmental advantages over conventional vapor compression refrigeration systems, primarily due to the exclusion of synthetic refrigerants that contribute to ozone depletion and global warming. Unlike conventional chillers that use hydrofluorocarbon (HFC) or hydrochlorofluorocarbon (HCFC) refrigerants with high (GWP) and (ODP), the LiBr absorption system uses water as the refrigerant, which has zero ODP and zero direct GWP, thereby eliminating refrigerant-related greenhouse gas emissions. The system achieves cooling through a thermally driven cycle rather than electrical compression, enabling integration with low-grade heat sources such as geothermal energy in the current case. Single-effect LiBr absorption chillers typically operate with generator temperatures in the range of 80–100°C and achieve coefficients of performance (COP) between 0.6 and 0.8 under standard operating conditions.

The climate impact benefits are further enhanced when absorption chillers are coupled with renewable or waste heat sources, as modeling studies have shown that utilizing low-grade heat in place of grid electricity or additional fuel combustion results in substantial reductions in the overall carbon footprint of cooling systems, improving primary energy utilization and reducing upstream emissions associated with electricity generation.

4.4.3 Hazard and Operability

Hazard and Operability (HAZOP) analysis of LiBr absorption chiller systems identifies crystallization of the lithium bromide solution as the primary operational hazard, as salt precipitation within the absorber, generator, or solution piping can block flow passages, disable heat transfer surfaces, and cause complete system shutdown. Crystallization occurs when the LiBr solution becomes supersaturated due to excessive concentration or inadequate temperature control, with risk increasing when absorber temperatures rise at fixed evaporator pressure conditions, when solution mass fractions exceed solubility limits, or when local cooling creates conditions that favor salt precipitation. The crystallization boundary is highly sensitive to absorber heat rejection effectiveness, solution concentration control, and ambient cooling water temperature, requiring careful design and operational controls to maintain solution conditions within the stable liquid region of the LiBr-H_2O phase diagram. Field experience and experimental studies have shown that crystallization events can occur during abnormal operating conditions such as cooling water supply interruptions, excessive generator heating, improper startup or shutdown procedures, or ambient temperature excursions that reduce absorber cooling effectiveness. The consequences of crystallization include immediate loss of cooling capacity, potential damage to pumps and heat exchangers due to solid deposits, extended downtime for system flushing and dilution procedures, and possible permanent damage to heat transfer surfaces if crystallized deposits are not promptly removed. HAZOP studies for LiBr systems must therefore include detailed examination of all operating scenarios that could lead to solution supersaturation, with particular attention to absorber temperature control, solution concentration monitoring, cooling water supply reliability, and emergency dilution procedures.

Corrosion and material degradation represent significant hazards in LiBr absorption chiller systems, particularly when seawater or aggressive cooling water sources are employed for heat rejection in the absorber and condenser units. The LiBr solution itself is corrosive to many common metals, and the presence of oxygen, moisture, and elevated temperatures accelerates corrosion rates, requiring careful material selection and the use of corrosion inhibitors to ensure long-term system integrity. In systems utilizing direct seawater cooling, the combination of saline water and LiBr solution creates a highly corrosive environment that necessitates the use of specialized materials such as titanium tubes, corrosion-resistant coatings, and protective barriers to prevent rapid degradation of heat exchanger surfaces. Field testing of a large-scale direct seawater-cooled absorption chiller employed titanium tubes, anticorrosive paints, and rubber covers for condenser and absorber surfaces to manage corrosion risks and extend equipment service life. The HAZOP analysis must address potential corrosion failure modes including heat exchanger tube perforation, solution contamination from corrosion products, reduced heat transfer effectiveness due to scale formation, and structural failure of pressure-containing components. Mitigation strategies include the use of corrosion-resistant materials (stainless steel, titanium, copper-nickel alloys), application of protective coatings and linings, addition of corrosion inhibitors to the LiBr solution (such as lithium chromate or lithium molybdate), regular monitoring of solution pH and corrosion product concentrations, and implementation of preventive maintenance programs that include periodic inspection and replacement of sacrificial components.

Beyond crystallization and corrosion, HAZOP analysis of LiBr absorption chillers must address several additional safety and operational hazards including pressure vessel integrity, thermal expansion risks, solution toxicity concerns, and system overpressure scenarios. The system operates under vacuum conditions in the evaporator and absorber sections (typically 0.7–1.2 kPa absolute pressure) and elevated pressures in the generator and condenser sections (typically 7–10 kPa absolute pressure for single-effect systems), requiring proper pressure vessel design, vacuum-tight construction, and pressure relief devices to prevent catastrophic failure or air ingress that would degrade performance. Although the supplied literature does not provide specific toxicological data for LiBr solution exposure limits, lithium bromide is known to be an irritant to skin, eyes, and respiratory systems, requiring appropriate personal protective equipment during maintenance operations, proper containment of solution spills, and emergency response procedures for solution releases. Additional hazards identified in HAZOP reviews include thermal expansion of solution and refrigerant streams, potential for generator overheating if heat input is not properly controlled, risks of pump cavitation or deadheading, and hazards associated with high-temperature surfaces and hot water supply systems. The system design must incorporate multiple layers of protection including temperature and pressure instrumentation with automatic shutdown interlocks, solution level monitoring and low-level alarms, flow monitoring for cooling water and hot water circuits, emergency dilution systems for crystallization events, and proper venting and purging procedures to remove non-condensable gases that amass during operation.

4.4.4 Economic Analysis

A comprehensive economic analysis of the Lithium Bromide absorption chiller system has been performed using Aspen Economic Analyzer to evaluate the capital investment requirements, operating costs, and overall economic viability of the geothermal-powered cooling system for data center applications. The economic evaluation encompasses detailed estimation of equipment purchase costs including the generator (flash separator), absorber, condenser, evaporator, solution heat exchangers (COLD, HX-1, HX-2, and HOT), solution circulation pump, expansion valves, and auxiliary systems such as cooling water circulation equipment and instrumentation. The analysis considers both direct costs (equipment, materials, installation labor) and indirect costs (engineering design, construction management, contingencies, startup and commissioning) to determine the total capital investment required for the absorption chiller facility. *Table 16* shows the overall cost of the process evaluated by Aspen Economic Analyzer.

Table 16. showing the economic analysis

Currency	USD	Euro
Total Capital Cost	4,167,120	3,508,298
Total Operating Cost [/Year]	6,605,270	5,560,976
Total Raw Materials Cost [USD/Year]	0	0
Total Utilities Cost [USD/Year]	5,243,000	4,414,081
Desired Rate of Return [Percent/'Year]	20	20
Equipment Cost [USD]	1,211,700	1,020,130
Total Installed Cost [USD]	2,593,600	2,183,551

Operating cost estimation includes energy consumption for pumping operations, cooling water supply and treatment costs, maintenance and inspection expenses, corrosion inhibitor and solution makeup costs, and labor requirements for system operation and supervision. The economic model also accounts for the avoided costs associated with eliminating conventional electric chiller equipment and the significant reduction in electrical energy consumption, as the absorption system utilizes the available 14 MW geothermal thermal energy rather than grid electricity for cooling production. Additional economic benefits include potential carbon credit revenues from avoided greenhouse gas emissions, reduced peak electrical demand charges, and improved energy security through utilization of the renewable geothermal resource. The detailed equipment's price along with their installation cost is tabulated below in *Table 17*, which also represents the weight of equipment before and after installation.

Table 17. Equipment costs of the absorption chiller

Name	Equipment Cost [$]	Equipment Cost [€]	Installed Cost [$]	Equipment Cost [€]	Equipment Wt. [lbs]	Installed Wt. [lbs]
Condenser	168,300	141,691	352,800	297,075	30,600	59,820
Heat Exchanger (HX-3)	11,400	9,597	81,200	68,374	500	6,382
Heat Exchanger (Cold)	23,000	19,363	109,000	91,783	2,900	13,008
Evaporator	28,300	23,825	135,900	114,434	4,000	19,255
Heat Exchanger (Hot)	45,300	38,138	166,500	140,201	7,100	24,709
Heat Exchanger (HX-2)	17,600	14,817	106,000	89,257	1,800	12,785
Heat Exchanger (HX-1)	11,300	9,515	72,800	61,301	450	5,932
Pump	12,000	10,104	81,800	68,879	560	9,173
Generator-flash vessel	61,000	51,365	307,300	258,761	11,500	38,075
Absorber	833,500	701,848	1,180,300	993,871	154,200	206,983
Total	1,211,700	1,020,263	2,593,600	2,183,936	213,600	396,122

4.5 Comparative analysis of ORC and LiBr Absorption Chiller for Cooling

A comparative analysis between the two investigated cooling approaches—Organic Rankine Cycle (ORC) coupled with electric chillers and a Lithium Bromide (LiBr) absorption chiller—clearly indicates the advantages of direct utilization of geothermal energy for data center cooling. The ORC system, modeled with dual iso-pentane loops, generates 1.4987 MW of electrical power, which drives electric chillers with a typical COP of 4.5, resulting in a total cooling output of 6.744 MW. In contrast, the LiBr absorption chiller directly converts the 14 MW of available geothermal thermal energy into cooling, producing a significantly higher cooling duty of 11.334 MW. Consequently, the absorption chiller achieves an overall thermal efficiency of approximately 81%, compared to 48% for the ORC-electric chiller system. Furthermore, the absorption system is less complex, requiring fewer moving parts and lower maintenance, while the ORC configuration involves multiple turbines, pumps, and heat exchangers, increasing operational and maintenance demands. These results demonstrate that, for direct geothermal cooling applications, the LiBr absorption chiller provides higher performance in terms of cooling capacity, energy efficiency, and system simplicity, whereas the ORC approach is only advantageous if electricity generation is also required.

Chapter 5: Hypothetical Data Center Design Utilizing the Absorption Chiller Cooling

With a cooling plant capacity of 11.334 MW, the engineering aim is to optimize the supported Information Technology (IT) load while reducing Power Usage Effectiveness (PUE) via a cohesive design that harmonizes mechanical refrigeration, electrical distribution, and state-of-the-art liquid cooling systems. This chapter offers an in-depth examination of the mechanical, electrical, and structural needs for enhancing such a facility, featuring a thorough breakdown of the supported IT capacity and anticipated efficiency indicators.

5.1 Computer Room Air Handling (CRAH)

To distribute 11.334 MW of cooling within the data hall, a strong network of Computer Room Air Handling (CRAH) units is necessary. In contrast to Computer Room Air Conditioning (CRAC) units that have internal compressors and refrigerants, CRAH units are advanced fan-coil units that utilize chilled water from the central plant [99]. This design enhances cooling density and decreases the count of moving parts in the white space, which reduces the likelihood of component failure. Larger capacity units (up to ~300kW per unit) suitable for moderate to large data halls [100]. So, by a simple calculation the total amount of CRAH units need is:

- Number of CRAHs = $\frac{11.334\ MW}{0.3\ MW}$ = 38 CRAH units [**Eq.32**]

In an actual measured data center, CRAH units consumed only about 9 % of the total electrical load, including fans and controls.

5.2 Uninterruptible Power Supply (UPS)

UPS systems are utilized in data centers to provide uninterrupted, stable, and clean electricity for delicate IT hardware. Their primary function is to deliver immediate backup power in the event of a utility supply failure, closing the gap between a grid outage and generator activation, preventing servers from shutting down suddenly, which could lead to data loss or system failures [101]. This safeguard aids in avoiding hardware harm and prolongs the lifespan of equipment. UPS systems enhance data center reliability levels by providing redundant power routes and allowing maintenance without interruptions. Nevertheless, since no UPS achieves 100% efficiency, around 5% of the IT load is dissipated as heat during the AC–DC–AC conversion, and this excess heat needs to be managed by the cooling system, which slightly raises the total cooling requirement [101].

5.3 Lighting Consumption in Data Centers

Although lighting usually represents only around 3% of a data center's overall energy consumption, it still plays a crucial role in ensuring safe and efficient operations [102]. Adequate lighting enables technicians to easily read equipment labels, identify cable routes, and understand floor plans during installations, maintenance tasks, and emergency situations. Clear visibility minimizes the chances of human mistakes, accelerates repair tasks, and enhances safety adherence. Contemporary data centers frequently utilize energy-efficient LED lighting equipped with occupancy and motion sensors, ensuring lights are primarily on when staff are available, reducing energy waste while preserving a secure workplace.

5.4 IT load Calculations

Under the assumption that only IT equipment, UPS losses, lighting, and CRAH units add to the heat load in the cooled area, the IT electrical load can be established via a steady-state energy balance. The overall cooling capacity of the data center is 11.334 MW, assumed to match the total heat released within the data hall. Let P_{IT} be the IT load and P_{tot} the total electrical load that ultimately becomes heat. UPS conversion losses account for 5% of the IT load ($0.05\,P_{IT}$), while lighting and CRAH units represent 3% and 9% of the total electrical load, respectively ($0.03\,P_{tot}$ and $0.09\,P_{tot}$). The total load can therefore be written as:

- $P_{tot} = P_{IT} + 0.05P_{IT} + 0.03P_{tot} + 0.09P_{tot}$ **[Eq.33]**

Since the cooling system removes all internally generated heat, $Q \approx P_{tot}$. Substituting $Q = 11.334$MW yields:

- $P_{IT} = \frac{11.334}{1.19318} \approx 9.5$ MW **[Eq.34]**

Therefore, the IT equipment load is approximately **9.5 MW**, with the remaining power attributable to UPS losses, lighting, and CRAH operation.

5.5 Power Usage Effectiveness of Data Center

Now using **[Eq.2]** of power usage effectiveness (PUE), we will get the following:

- $PUE = \frac{11.334}{9.5} = 1.19$

A PUE value of 1.19 reflects a significant degree of energy efficiency within the 9.5 MW data center which is counted as medium to large facility. This indicates that for each 1 kW of power used by IT devices, another 0.19 kW is necessary to run supporting infrastructure, including cooling systems, power conversion devices, and lighting. About 84% of the overall electrical energy that enters the facility is directly utilized by IT equipment, with the other 16% being used by supporting systems. This indicates an effective facility layout, as the PUE value approaches the optimal figure of 1.0, representing a theoretical scenario where all provided power is utilized solely for IT functions without any excess.

By comparing the average PUE for Italy (=1.48) with the one calculated for Ferrara Data Center (=1.19), and the Italian average emission factor (310 kg/MWh) with the one estimated for the LiBr-H2O absorption chiller hypothesized for Ferrara, expected reductions in the annual energy needs and CO2 emissions are estimated at 24,134 MWh and 7,481 tons, respectively (*Figure 27*).

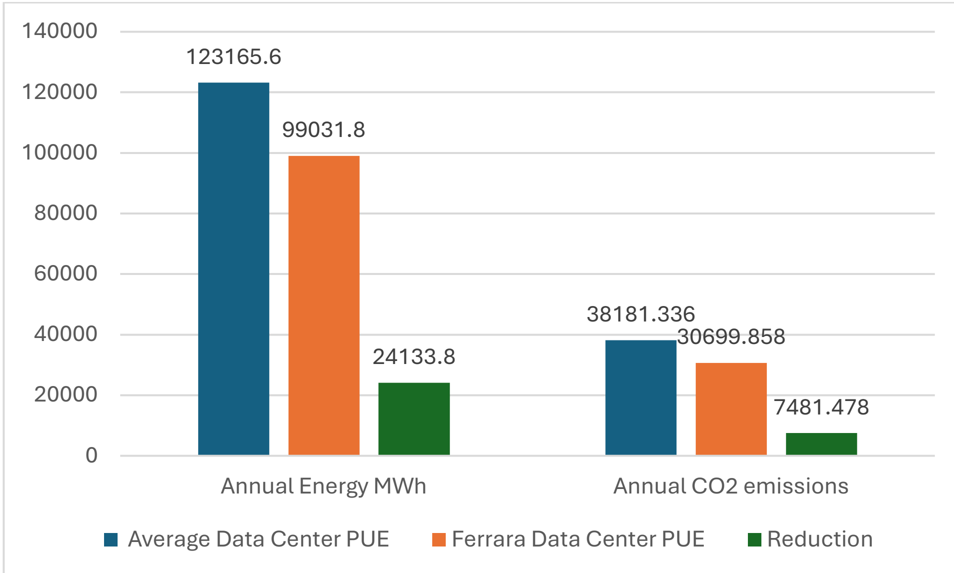

Figure 27. Annual energy (MWh) and CO2 emssions (Tons) between the Italian averaged Data Centers and hypothetical ferrara Fata Center'

Based on these results which are calculated for same IT load data centers which is 9.5 MW, we observe that the usage of geothermal absorption chiller will decrease the PUE value from 1.48 to 1.19 due to less energy consumption in cooling process, which yields 20% reduction in the annual energy consumption and CO2 emissions.

6. Conclusion

The Ferrara Geothermal System demonstrates strong potential for direct integration with a single-effect lithium bromide (LiBr) absorption chiller to provide cooling for data center applications. The geothermal resource delivers 14 MW of thermal energy at 100°C with a flow rate of 400 m^3/hr, fully meeting the generator temperature requirements of single-effect absorption systems. This makes it highly suitable for driving heat-driven cooling without reliance on grid electricity or fossil fuels.

Compared to alternatives such as organic Rankine cycle (ORC) systems, the LiBr absorption chiller achieves significantly higher cooling output, maximizing the utilization of renewable thermal energy. By leveraging geothermal heat, the system reduces primary energy consumption and carbon emissions, offering clear environmental and operational advantages.

Lifecycle assessments and integration modeling indicate that geothermal-powered absorption cooling can substantially lower system-level carbon footprints while maintaining high energy efficiency. These benefits position direct geothermal-driven absorption cooling as a technically feasible, energy-efficient, and environmentally sustainable solution for energy-demanding digital infrastructures.

Future research should explore hybrid configurations, seasonal thermal storage, and absorption cycle optimization to further enhance system performance, adaptability, and overall sustainability.

Reference List

1. European Commission. (n.d.). *Geothermal energy*. Energy. https://energy.ec.europa.eu/topics/renewable-energy/geothermal.energy_en#:~:text=Geothermal%20energy%20is%20a%20renewable,%C2%A9%20European%20Union%2C%202020
2. International Energy Agency. (2024). *The future of geothermal energy*. IEA. https://www.iea.org/reports/the-future-of-geothermal-energy
3. Mjami, N. B., Kimambo, C., Ayeng'o, S., & Orozova-Bekkevold, I. (2025). Prospects and challenges for utilisation of low- to medium-temperature geothermal resources in Tanzania. *Geothermics, 129,* 103288. https://doi.org/10.1016/j.geothermics.2025.103288
4. Anya, B., Mohammadpourfard, M., Akkurt, G. G., & Mohammadi-Ivatloo, B. (2024). Exploring geothermal energy-based systems: Review from basics to smart systems. *Renewable and Sustainable Energy Reviews, 210,* 115185. https://doi.org/10.1016/j.rser.2024.115185
5. International Renewable Energy Agency. (2023, February 1). *Global geothermal market and technology assessment*. https://www.irena.org/Publications/2023/Feb/Global-geothermal-market-and-technology-assessment
6. National Renewable Energy Laboratory. (2024). *Advancing geothermal research: Fiscal year 2024 accomplishments report*. https://research-hub.nrel.gov/en/publications/advancing-geothermal-research-fiscal-year-2024-accomplishments-re/
7. Eze, V. H. U., Eze, E. C., Alaneme, G. U., & Bubu, P. E. (2025). Recent progress and emerging technologies in geothermal energy utilization for sustainable building heating and cooling: A focus on smart system integration and enhanced efficiency solutions. *Frontiers in Built Environment, 11.* https://doi.org/10.3389/fbuil.2025.1594355
8. International Energy Agency. (2024). *The future of geothermal energy*. https://www.iea.org/reports/the-future-of-geothermal-energy
9. U.S. Energy Information Administration. (2023). *Industrial sector energy consumption*. https://www.eia.gov/outlooks/ieo/pdf/industrial.pdf
10. Data center infrastructure: 5 key components and best practices. Available at: https://www.instaclustr.com/education/data-architecture/data-center-infrastructure-5-key-components-and-best-practices/
11. Clean Energy Forum. (2025, November 12). *Data center energy consumption: How much energy did/do/will they eat?* https://cleanenergyforum.yale.edu/2025/11/12/data-center-energy-consumption-how-much-energy-diddowill-they-eat
12. De Chant, T. (2025, December 1). Data center energy demand forecasted to soar nearly 300% through 2035. *TechCrunch.* https://techcrunch.com/2025/12/01/data-center-energy-demand-forecasted-to-soar-nearly-300-through-2035/
13. Structure Research. (2025). *ESG report: Data centre environmental impact.* https://dcnnmagazine.com/data-centres/2025-esg-report-data-centre-environmental-impact/
14. Mytton, D. (2021). Data centre water consumption. npj Clean Water, 4, Article 11. https://doi.org/10.1038/s41545-021-00101-w

15. ProChem Water. (2025, November 10). Do data centers recycle water? How they do it efficiently. ProChem Water. https://www.prochemwater.com/blog/water-efficiency-reuse/do-data-centers-recycle-water
16. Hegde, G. (2026, January 23). Myths vs. reality: Data centers and water usage. Florida Water & Pollution Control Operators Association. https://www.fwpcoa.org/content.aspx?club_id=859275&item_id=130961&page_id=5
17. Grand View Research. (2024). *Data center market size and share | Industry report, 2030.* https://www.grandviewresearch.com/industry-analysis/data-center-market-report
18. International Energy Agency. (2023). *District heating – Energy system.* https://www.iea.org/energy-system/buildings/district-heating
19. International Renewable Energy Agency (IRENA). (n.d.). Power to heat and cooling: Status. Innovation landscape for smart electrification. Retrieved from https://www.irena.org/Innovation-landscape-for-smart-electrification/Power-to-heat-and-cooling/Status
20. Global Market Statistics. (2024). *District heating and cooling market report.* https://www.globalmarketstatistics.com/market-reports/district-heating-and-cooling-market-12402
21. Grand View Research. (2024). *District heating market report.* https://www.grandviewresearch.com/industry-analysis/district-heating-market-report
22. United Nations Environment Programme. (2025). Global Cooling Watch 2025. UNEP. Retrieved from https://www.unep.org/resources/global-cooling-watch-2025
23. Eveloy, V., & Ayou, D. S. (2019). Sustainable district cooling systems: Status, challenges, and future opportunities, with emphasis on cooling-dominated regions. *Energies, 12*(2), 235. https://doi.org/10.3390/en12020235
24. Fortune Business Insights. (2025). *District cooling market size, share & industry analysis, by technology, by end-user, and regional forecast, 2025–2032.* https://www.fortunebusinessinsights.com/industry-reports/district-cooling-market-100090
25. Amiad Water Systems. (n.d.). Seawater desalination system: Processes, technologies, and key challenges. Retrieved December 3, 2025, from https://amiad.com/solutions/seawater-desalination-system/
26. Chebli, H., Fornarelli, F., & Bellantuono, N. (2023). Comparison of desalination technologies and assessment of their sustainability. Journal of Physics: Conference Series, 2648(1), 012021. https://doi.org/10.1088/1742-6596/2648/1/012021
27. Eyl-Mazzega, M.-A., & Cassignol, É. (2022). The geopolitics of seawater desalination. Études de l'Ifri. Ifri. https://www.ifri.org/en/studies/geopolitics-seawater-desalination
28. Wang, Y., Morosuk, T., & Cao, W. (2024). Carbon footprint of seawater desalination technologies: A review. Journal of Energy Resources Technology, 146(8), 080801. https://doi.org/10.1115/1.4065251
29. International Energy Agency (IEA). (2024). Energy demand for desalination in the Stated Policies Scenario, 1990–2030. IEA. https://www.iea.org/data-and-statistics/charts/energy-demand-for-desalination-in-the-stated-policies-scenario-1990-2030
30. Global Clean Water Desalination Alliance. (2015). H_2O minus CO_2: Concept paper. Columbia University. Retrieved from http://www.clca.columbia.edu/Global-Water.pdf

31. Business Research Insights. (2025). Desalination market size, share, growth, and industry analysis, by type, application, and regional forecast to 2033. Retrieved from https://www.businessresearchinsights.com/market-reports/desalination-market-120534
32. Olabi, A. G., Elsaid, K., Rabaia, M. K. H., Askalany, A. A., & Abdelkareem, M. A. (2020). Waste heat-driven desalination systems: Perspective. Energy, 209, Article 118373. https://doi.org/10.1016/j.energy.2020.118373
33. Directorate-General for Environment. (2026, March 30). AI data centre waste heat could be used for water purification and carbon capture. European Commission – Environment. https://environment.ec.europa.eu/news/ai-data-centre-waste-heat-could-be-used-water-purification-and-carbon-capture-2026-03-30_en
34. GHD. (2025, August 27). *The role of geothermal energy in the industrial energy transition: A multi-technology solution.* https://www.ghd.com/en-us/insights/the-role-of-geothermal-energy-in-the-industrial-energy-transition-a-multi-technology-solution
35. International Geothermal Association. (2020). Olkaria Green Energy Park case study. In *Proceedings of the World Geothermal Congress 2020.* https://www.worldgeothermal.org/pdf/IGAstandard/WGC/2020/38001.pdf
36. Kearney Energy Transition Institute. (2025). *Geothermal FactBook: Turning up the heat.* https://www.energy-transition-institute.com/documents/d/eti/kearney-eti-geothermal-factbook-2025-pdf
37. Geosyn. (2025, November 26). *Geosyn Project - Geothermal Synergy.* https://geosynproject.eu/
38. Oqubay, A., & Lin, J. Y. (2020). Industrial hubs and economic development: An introduction. In The Oxford Handbook of Industrial Hubs and Economic Development (pp. 1–24). Oxford University Press. https://doi.org/10.1093/oxfordhb/9780198850434.013.1
39. Gereffi, G., & Wu, X. (2020). Global value chains, industrial hubs, and economic development in the twenty-first century. In A. Oqubay & J. Y. Lin (Eds.), The Oxford Handbook of Industrial Hubs and Economic Development (pp. 1049–1068). Oxford University Press. https://doi.org/10.1093/oxfordhb/9780198850434.013.53.
40. World Bank. (2023). Benchmarking Infrastructure Development 2023: Assessing regulatory quality to prepare, procure, and manage PPPs in infrastructure projects. World Bank Group. https://bpp.worldbank.org/en/home
41. United Nations Industrial Development Organization. (2020). Industrial Development Report 2020: Industrializing in the digital age. Vienna: UNIDO. https://www.unido.org/resources/publications/industrial-development-report-series/idr2020
42. International Labour Organization & Eurofound. (2019). Working conditions in a global perspective. Luxembourg: Publications Office of the European Union; Geneva: International Labour Organization. https://www.ilo.org/sites/default/files/wcmsp5/groups/public/@dgreports/@dcomm/@publ/documents/publication/wcms_696174.pdf.
43. Italy and Geothermal Energy: a centre of excellence with historic roots. (2025, October 17). Opportunitaly. https://opportunitaly.gov.it/news-and-media/geothermal-energy-italy-excellence
44. European Geothermal Energy Council. (2018). Potential and prospects for geothermal energy development in Italy. https://www.egec.org/wp-content/uploads/post/Potential-and-prospects-for-geothermal-energy-development-in-Italy.pdf
45. Richter, A. (2022, July 8). Geothermal electricity production in Italy with 115 TWh potential. ThinkGeoEnergy. https://www.thinkgeoenergy.com/geothermal-electricity-production-in-italy-with-115-twh-potential/

46. Cataldi, R., Mongelli, F., Squarci, P., Taffi, L., Zito, G., & Calore, C. (2000). Geothermal ranking of Italian territory. Geothermics, 24(1), 115-IN6. https://doi.org/10.1016/0375-6505(94)00026-9
47. Tenaris. (2025, January 13). Tenaris highlights 30 years of supporting the Larderello geothermal site in Italy. ThinkGeoEnergy. Retrieved from https://www.thinkgeoenergy.com/tenaris-highlights-30-years-of-supporting-the-larderello-geothermal-site-in-italy/
48. Enel Green Power. (n.d.). The "Valle Secolo" geothermal power plant in Larderello, Italy. Retrieved January 15, 2026, from https://www.enelgreenpower.com/our-projects/operating/geothermal-power-plant-larderello
49. Minissale, A. (1991). The Larderello geothermal field: A review. Geothermics, 20(1-2), 15–29. Retrieved from https://www.researchgate.net/profile/Angelo-Minissale/publication/223771915_The_Larderello_geothermal_field_a_review/links/5aa25ea10f7e9badd9a60e74/The-Larderello-geothermal-field-a-review.pdf
50. Liotta, D., Brogi, A., & Gianelli, G. (2025). The progress of geothermal knowledge at Larderello: A review of structural, thermal, and fluid evolution. Italian Journal of Geosciences, 144(2), 228–247. https://doi.org/10.3301/IJG.2025.02
51. Batini, F., Gianelli, G., & Pandeli, E. (1983). Deep drilling in Larderello field: Results and implications. Geothermics, 12(2–3), 141–151. https://doi.org/10.1007/BF00320975
52. Bellani, S., & Gherardi, F. (2007). Geothermal exploration in Larderello-Travale area: Recent developments and perspectives. Geothermal Resources Council Transactions, 31, 103–574. Retrieved from https://www.publications.mygeoenergynow.org/grc/1030574.pdf
53. Arias, A., Romagnoli, P., Barelli, A., Ceccarelli, A., & Fiordelisi, A. (2010). Larderello-Travale geothermal system: Reservoir characterization and modeling. Proceedings World Geothermal Congress 2010, Bali, Indonesia, 25–29 April 2010. Retrieved from https://pangea.stanford.edu/ERE/db/IGAstandard/record_detail.php?id=5972
54. Batini, F., Gianelli, G., & Pandeli, E. (1985). Deep drilling in the Larderello geothermal field: Results and implications. In L. Rybach & L.J.P. Muffler (Eds.), Geothermal Systems: Principles and Case Histories (pp. 331–364). Springer. https://doi.org/10.1007/978-94-009-3691-1_16
55. Kumar, S. (2025, July 24). Geothermal district heating in Ferrara — Geothermal stories. Geothermal Stories. https://www.geothermalstories.org/stories1/Blog%20Post%20Title%20One-s26wg-aeyr4
56. European Geothermal Energy Council. (n.d.). Ferrara geothermal district heating. Retrieved from https://www.egec.org/publications/ferrara-geothermal-district-heating/
57. Metropolitan City of Bologna. (2021). Invest in Bologna: Your future home [Brochure]. Invest in Bologna. https://www.investinbologna.it/Engine/RAServeFile.php/f/Brochure_ENG_def16072021.pdf
58. Prologis. (n.d.). Bologna, one of Europe's most important logistics and intermodal platform. Prologis. https://www.prologis.it/en/properties/bologna-one-europes-most-important-logistics-and-intermodal-platform
59. Favero, S. (2023). Idrovia Padova-Venezia: infrastruttura multifunzionale per la mobilità sostenibile e la mitigazione del rischio idraulico [Bachelor's thesis, University of Padua]. Padua Thesis and Dissertation Archive. https://hdl.handle.net/20.500.12608/71490

60. Regione del Veneto. (n.d.). PREPAIR: Caso studio Veneto. https://www.regione.fvg.it/rafvg/export/sites/default/RAFVG/ambienteterritorio/energia/FOGLIA112/allegati/PREPAIR_Caso_studio_Veneto.pdf
61. Wikipedia contributors. (n.d.). Alfa Romeo Pomigliano d'Arco plant. In Wikipedia, The Free Encyclopedia. Retrieved January 21, 2026, from https://en.wikipedia.org/wiki/Alfa_Romeo_Pomigliano_d%27Arco_plant
62. Interporto Campano S.p.A. (n.d.). Interporto Campano is one of Europe's main logistics facilities [Company profile]. Interporto Campano. https://www.interportocampano.it/en/company-profile-en/
63. International Union of Railways. (2017, June 27). Italy: Prime Minister Paolo Gentiloni opens the new Napoli Afragola station. UIC Communications. https://www.uic.org/com/enews/nr/554/article/italy-prime-minister-paolo-gentiloni-opens-the-new-napoli-afragola-station
64. Azevedo, F. (2015). Economic, social and territorial situation of Sicily (In-depth analysis, PE 540.372). European Parliament, Policy Department B: Structural and Cohesion Policies. https://www.europarl.europa.eu/cmsdata/120267/pe540372_en.pdf
65. Wikipedia contributors. (n.d.). Palermo. In Wikipedia, The Free Encyclopedia. Retrieved January 22, 2026, from https://en.wikipedia.org/wiki/Palermo
66. Pigliucci, M. (Ed.). (2025). Special Economic Zones: Challenges and Opportunities for Territorial Development (Vol. 8, No. 1). Il Sileno Edizioni. https://www.researchgate.net/publication/396523705_Special_Economic_Zones_Challenges_and_Opportunities_for_Territorial_Development
67. Azevedo, F. (2015). Economic, social and territorial situation of Sicily (In-depth analysis, PE 540.372). European Parliament, Policy Department B: Structural and Cohesion Policies. https://www.europarl.europa.eu/cmsdata/120267/pe540372_en.pdf
68. Wikipedia contributors. (n.d.). Sciacca. In Wikipedia, The Free Encyclopedia. Retrieved January 22, 2026, from https://en.wikipedia.org/wiki/Sciacca
69. European Sea Ports Organisation. (2025, December 18). Port Pro of the Month: Annalisa Tardino (IT). ESPO. https://www.espo.be/news/port-pro-of-the-month-annalisa-tardino-it
70. Bompan, E., & Rota, M. C. (2025, November 21). Energy and WEEE, data centres are at the forefront of a circular economy. Ecomondo. https://www.ecomondo.com/en/news-detail/energy-and-weee-data-centres-are-at-the-forefront-of-a-circular-economy?newsId=5839395
71. Lardizabal, E. (2025, April 9). Italy projects 30% annual growth in data centres for the next five years: A strategic signal for the renewable energy sector. StrategicEnergy.eu. https://strategicenergy.eu/italy-data-centres/
72. Vegni, C. (2025, April 17). Rising in the intelligent age: Milan's tech revolution. Equinix Blog. https://blog.equinix.com/blog/2025/04/17/rising-in-the-intelligent-age-milans-tech-revolution/
73. Fiordalisi, M. (2025, July 17). Data center, in Italia si rischiano cattedrali nel deserto. Wired Italia. https://www.wired.it/article/data-center-italia-cattedrali-nel-deserto/
74. Ministero delle Imprese e del Made in Italy. (2025). Strategia per l'attrazione in Italia degli investimenti industriali esteri in Centri Dati (Data Center). https://www.mimit.gov.it/images/stories/documenti/ATTRAZIONE_DEI_DATA_CENTER_2025.pdf

75. Greenreport. (2025, October 31). Data center, la potenza installata in Italia triplicherà fino a 2GW entro i prossimi cinque anni. Retrieved January 14, 2026, from https://www.greenreport.it/news/scienza-e-tecnologie/58553-data-center-la-potenza-installata-in-italia-triplichera-fino-a-2gw-entro-i-prossimi-cinque-anni
76. Nowtricity. (n.d.). CO_2 emissions per kWh in Italy. Retrieved January 14, 2026, from https://www.nowtricity.com/country/italy/
77. Terna Lightbox. (2025, August 8). Data centres and the future: the energy challenge facing Italy. Retrieved January 14, 2026, from https://lightbox.terna.it/en/insight/data-center-trasmission-grid
78. Cloudscene. (n.d.). Italy | Data center market overview. Cloudscene. Retrieved January 14, 2026, from https://cloudscene.com/market/data-centers-in-italy/all
79. Data Center Map. (n.d.). Noovle DC Roma data center – Rome, Italy. Retrieved January 14, 2026, from https://www.datacentermap.com/italy/rome/noovle-roma/
80. Jiménez-García, J. C., Ruiz, A., Pacheco-Reyes, A., & Rivera, W. (2023). A comprehensive review of organic Rankine cycles. Processes, 11(7), 1982. https://doi.org/10.3390/pr11071982
81. Mustapić, N., Brkić, V., Duić, Ž., & Kralj, T. (2022). Thermodynamic optimization of advanced Organic Rankine Cycle configurations for geothermal energy applications. Energies, 15(19), 6990. https://doi.org/10.3390/en15196990
82. Fu, W., Chen, J., & Yao, T. (2017). Optimization of Organic Rankine Cycle using low and medium temperature heat sources in Kenya. GRC Transactions, 41 https://publications.mygeoenergynow.org/grc/1033880.pdf
83. Laghari, A. S., Chandio, M. W., Kumar, L., & El Haj Assad, M. (2024). Thermodynamic performance analysis of geothermal power plant based on Organic Rankine Cycle (ORC) using mixture of pure working fluids. Energy Engineering, 121(8), 1–10. https://doi.org/10.32604/ee.2024.051082
84. Climeon. (n.d.). ORC technology. https://climeon.com/orc-technology/
85. Kaczmarczyk, M., Sowiżdżał, A., & Tomaszewska, B. (2024). Life cycle and water footprint assessment in the geothermal energy sector. Energies, 17(23), 6050. https://doi.org/10.3390/en17236050
86. Fervo Energy. (2025, March 31). Geothermal mythbusting: Water use and impacts. https://fervoenergy.com/geothermal-mythbusting-water-use-and-impacts/
87. U.S. Geological Survey. (2019, March 1). Thermoelectric power water use. https://www.usgs.gov/mission-areas/water-resources/science/thermoelectric-power-water-use
88. Zhao, H., Xu, H., Jin, D., & An, W. (2024). Research on geothermal-driven single-effect absorption refrigeration systems with different working fluids: Energy and exergy analysis. International Journal of Low-Carbon Technologies, 19, 1689–1698. https://doi.org/10.1093/ijlct/ctae100
89. Alhuyi-Nazari, M., Mukhtar, A., Md Yasir, A. S. H., Ahmadi, M. H., Kumar, R., & Luong, T. N. L. (2024). Applications of geothermal sources for absorption chillers as efficient and clean cooling technologies for buildings: A comprehensive review. Journal of Building Engineering, 82, 108340. https://doi.org/10.1016/j.jobe.2023.108340
90. Clarion Energy Content Directors. (2018, August 29). The new era of absorption chillers. POWER Engineering. https://www.power-eng.com/operations-maintenance/the-new-era-of-absorption-chillers/
91. District heating carries geothermal energy into homes, thereby reducing fossil fuel consumption. (2026). Enel.com. https://www.enel.com/learning-hub/renewables/geothermal-energy/district-heating

92. Brown, C. S., Cassidy, N. J., Egan, S. S., & Griffiths, D. (2022). Thermal and Economic Analysis of Heat Exchangers as Part of a Geothermal District Heating Scheme in the Cheshire Basin, UK. Energies, 15(6), 1983. https://doi.org/10.3390/en15061983
93. Goldstein, B., Hiriart, G., & Blackwell, D. (n.d.). 4 Geothermal Energy Coordinating Lead Authors: Contributing Authors. https://www.ipcc.ch/site/assets/uploads/2018/03/Chapter-4-Geothermal-Energy-1.pdf
94. Carbon Independent. (2007). Emissions from home energy use. Www.carbonindependent.org. https://www.carbonindependent.org/15.html
95. Reducing Data Center Peak Cooling Demand and Energy Costs With Underground Thermal Energy Storage | NREL. (2025). Nrel.gov. https://www.nrel.gov/news/detail/program/2025/reducing-data-center-peak-cooling-demand-and-energy-costs-with-underground-thermal-energy-storage
96. CORDIS, cordis.europa.eu. (1999, October 21). TOWN DISTRICT HEATING USING GEOTHERMAL ENERGY [STAGE 1]. CORDIS | European Commission. https://cordis.europa.eu/project/id/GE.-00021-80
97. Workshop on GEOTHERMAL ENERGY STATUS AND FUTURE IN THE Peri -Adriatic Area "THE INTEGRATED FERRARAR PLANT" (50% Geothermal) 2. (2014). https://www.fondazioneinternazionale.org/wp-content/uploads/2014/08/2014_Buscaroli_GruppoHERA_Bologna-IT.pdf
98. HVAC Systems Encyclopedia. (n.d.). Chiller performance analysis for HVAC engineers. Ingener. Retrieved April 3, 2026, from https://ingener.by/technical-guides/chiller-performance-analysis/
99. Soh, C. (2025, July 16). Understanding data center cooling technology: From legacy systems to high-density solutions. Mitsubishi Critical. https://mitsubishicritical.com/resources/blog/types-of-data-center-cooling-technology/
100. Trane Technologies. (n.d.). Computer Room Air Handler for Data Centers (CRAH unit). Trane. Retrieved January 27, 2026, from https://www.trane.com/commercial/north-america/us/en/products-systems/airside-equipment/air-handlers-for-data-centers/crah-unit.html
101. ENERGY STAR. (n.d.). Reduce energy loss from uninterruptible power supply systems. U.S. Environmental Protection Agency. Retrieved January 27, 2026, from https://www.energystar.gov/products/data_center_equipment/16-more-ways-cut-energy-waste-data-center/reduce-energy-losses-uninterruptible-power-supply-ups-systems
102. Kleyman, B. (2014, April 24). Data center lighting and efficiency. Data Center Knowledge. Retrieved from https://www.datacenterknowledge.com/infrastructure/data-center-lighting-and-efficiency